UNIVERSITY OF SOUTH BOHEMIA IN ČESKÉ BUDĚJOVICE
FACULTY OF SCIENCE

Integrated structural study of the FrpD protein from *Neisseria meningitidis*

Ph.D. THESIS

Ekaterina Sviridova, MSc

Supervisor: Doc. Mgr. Ivana Kuta Smatanova, Ph.D.
University of South Bohemia in České Budějovice, Faculty of Science

České Budějovice 2016

This thesis should be cited as:
Sviridova E., 2016: Integrated structural study of the FrpD protein from *Neisseria meningitidis*. Ph.D. Thesis Series, No. 5. University of South Bohemia, Faculty of Science, České Budějovice, Czech Republic, 131 pp.

Annotation

Neisseria meningitidis (*N. meningitidis*) is a Gram-negative commensal bacterium colonizing nasopharynx of about 10 % of healthy individuals, which can cause invasive diseases, such sepsis and meningitis, upon occasional penetration into bloodstream. Pathogenesis of *N. meningitidis* appears to be directly related to conditions of limited iron availability. Under these conditions two proteins of unknown function: FrpC and FrpD, are synthesized. FrpD is a highly conserved lipoprotein of *N. meningitidis* anchored to the bacterial outer membrane. It is known that FrpD tightly binds the FrpC protein, which belongs to the Repeat-in-Toxin (RTX) protein family and may act as bacterial exotoxin. However, the mechanism of FrpD-FrpC interaction and the exact function of this complex are unknown due to the absence of structural information on these proteins. Therefore, we set out to determine the structure of FrpD and provide insights into its interaction mechanism with FrpC and structure-functional relationships of these two proteins.

We determined the first crystal and solution structures of the FrpD protein. We found that atomic structures of FrpD reveal a novel protein fold. We uncovered the structure-function relationships underlying the mechanism of interaction between the FrpD and FrpC proteins and tested the putative function of the FrpD-$FrpC_{1\text{-}414}$ complex *in vitro*. Finally, we proposed the putative function of the FrpD-$FrpC_{1\text{-}414}$ complex as a new minor adhesin of *N. meningitidis*, which mediates the bacterial adhesion to the host epithelial cells and facilitate the colonization. Our work constitutes the first step in clarifying the molecular basis of the FrpD-FrpC interaction and sets the base for further investigation of the role of FrpD and FrpC in the virulence mechanism of *N. meningitidis*.

Declaration [in Czech]

Prohlašuji, že svoji disertační práci jsem vypracovala samostatně pouze s použitím pramenů a literatury uvedených v seznamu citované literatury.

Prohlašuji, že v souladu s § 47b zákona č. 111/1998 Sb. v platném znění souhlasím se zveřejněním své disertační práce, a to v úpravě vzniklé vypuštěním vyznačených částí archivovaných Přírodovědeckou fakultou elektronickou cestou ve veřejně přístupné části databáze STAG provozované Jihočeskou univerzitou v Českých Budějovicích na jejích internetových stránkách, a to se zachováním mého autorského práva k odevzdanému textu této kvalifikační práce. Souhlasím dále s tím, aby toutéž elektronickou cestou byly v souladu s uvedeným ustanovením zákona č. 111/1998 Sb. zveřejněny posudky školitele a oponentů práce i záznam o průběhu a výsledku obhajoby kvalifikační práce. Rovněž souhlasím s porovnáním textu mé kvalifikační práce s databází kvalifikačních prací Theses.cz provozovanou Národním registrem vysokoškolských kvalifikačních prací a systémem na odhalování plagiátů.

České Budějovice, 30.06.2016

Ekaterina Sviridova

This thesis originated from the Faculty of Science, University of South Bohemia, supporting doctoral studies in the Biophysics study programme.

Financial support

This research was supported by the Czech Science Foundation grant P207/11/0717.

The thesis is based on the following publications:

I. **Ekaterina Sviridova**, Ladislav Bumba, Pavlina Rezacova, Katerina Prochazkova, Daniel Kavan, Karel Bezouska, Michal Kuty, Peter Sebo and Ivana Kuta Smatanova (2010) Crystallization and preliminary crystallographic characterization of the iron-regulated outer membrane lipoprotein FrpD from *Neisseria meningitidis*. *Acta Crystallographica Section F*, 66, 1119–1123. (IF = 0.60)

II. Ladislav Bumba, **Ekaterina Sviridova**, Ivana Kuta Smatanova, Pavlina Rezacova, Vaclav Veverka (2012) Backbone resonance assignments of the outer membrane lipoprotein FrpD from *Neisseria meningitidis*. *Biomolecular NMR Assignments*, 8 (1), 53–55. (IF = 0.82)

III. **Ekaterina Sviridova**, Pavlina Rezacova, Alexey Bondar, Vaclav Veverka, Petr Novak, Gundolf Schenk, Dmitri I. Svergun, Ivana Kuta Smatanova, and Ladislav Bumba. Structural basis of the interaction between the iron-regulated FrpD and FrpC proteins, putative minor adhesins of *Neisseria meningitidis*. *Manuscript*.

Publication not included in the thesis:

IV. Tatyana Prudnikova, Jose A. Gavira, Pavlina Rezacova, Estela Pineda Molina, Ivana Hunalova, **Ekaterina Sviridova**, Volha Shmidt, Jaroslava Kohoutova, Michal Kuty, David Kaftan, Frantisek Vacha, Juan Manuel Garcia-Ruiz and Ivana Kuta Smatanova (2010) Toward the crystallization of photosystem II core complex from *Pisum sativum* L. *Crystal Growth & Design*, 10, 3391–3396. (IF = 4.60)

Letter of declaration

Prohlašuji, že se Ekaterina Sviridova podílela na společných publikacích přibližně v níže uvedeném rozsahu.

I. **Ekaterina Sviridova**, Ladislav Bumba, Pavlina Rezacova, Katerina Prochazkova, Daniel Kavan, Karel Bezoushka, Michal Kuty, Peter Sebo and Ivana Kuta Smatanova (2010) Crystallization and preliminary crystallographic characterization of the iron-regulated outer membrane lipoprotein FrpD of *Neisseria meningitidis*. *Acta Crystallographica Section F*, 66, 1119–1123. (IF = 0.60)
ES conceived the idea (jointly with IKS and LB), performed protein purification experiments (jointly with LB), conducted crystallization and diffraction data collection experiments, analyzed the diffraction data (jointly with PR) and wrote the manuscript.

II. Ladislav Bumba, **Ekaterina Sviridova,** Ivana Kuta Smatanova, Pavlina Rezacova, Vaclav Veverka (2012) Backbone resonance assignments of the outer membrane lipoprotein FrpD from *Neisseria meningitidis*. *Biomolecular NMR Assignments*, 8 (1), 53–55. (IF = 0.82)
ES conceived the idea (jointly with PR and VV) and conducted protein preparation experiments (jointly with LB)

III. **Ekaterina Sviridova**, Pavlina Rezacova, Alexey Bondar, Vaclav Veverka, Petr Novak, Gundolf Schenk, Dmitri I. Svergun, Ivana Kuta Smatanova, and Ladislav Bumba. Structural basis of the interaction between the iron-regulated FrpD and FrpC proteins, putative minor adhesins of *Neisseria meningitidis. Manuscript.*
ES conceived the idea (jointly with IKS, LB and PR), conducted protein preparation experiments (jointly with LB), conducted crystallization and diffraction data collection experiments, analyzed the diffraction data (jointly with PR), performed SAXS experiments and wrote the manuscript.

Doc. Mgr. Ivana Kuta Smatanova, Ph.D.

Dedicated to my family

ACKNOWLEDGEMENTS

First of all I am deeply grateful to my beloved husband Alexey Bondar and son Arkadij, who have provided me with love and support.

I gratefully thank my supervisor Dr. Ivana Kuta Smatanova for her great help and support of my research. I would like to express my gratitude to Ivana for her ability to create a pleasant working atmosphere in our laboratory and for giving me possibility to cooperate with many other laboratories in the Czech Republic. I am also thankful to her for giving me the possibility to attend a lot of very useful structural biology courses and international conferences during my PhD studies.

I sincerely thank my scientific advisors Dr. Pavlina Rezacova and Dr. Ladislav Bumba who both helped and inspired me during the work on this very interesting project. I thank Dr. Ladislav Bumba for his help with protein preparation and characterization. I thank Dr. Pavlina Rezacova for introducing me the world of structural biology and her great help during all steps of my study. I also want to thank all my collegues who contributed to my work, especially Dr. Katerina Prochazkova, Dr. Jiry Brynda and Dr. Vaclav Veverka. I want to thank Dr. Uwe Mueller and Dr. Karthik Paithankar for their assistance with data collection at BESSY MX 14.1 beamline. I want to thank Dr. Dmitri Svergun, Dr. Gundolf Schenk and Dr. Clement Blanchet for their help with SAXS.

I am grateful Prof. Rudiger Ettrich and Prof. Peter Sebo for their indispensable support of my research.

I am grateful to Daniela Hambergerova and Dasha Kaftanova for their excellent assistance with all kinds of administrative issues.

I would like to thank all people who helped me during my PhD study, to my friends and colleagues from Nove Hrady, Ceske Budejovice and Prague, who made my life and work pleasant and enjoyable.

Finally, I am very grateful to all my family, my grandparents Tamara and Visilij, my aunt Svetlana, my parents in law Yuri and Natalia Bondar for their constant support, kind attention and invaluable help with Arkadij.

TABLE OF CONTENTS

LIST OF ABBREVIATIONS

2D – two-dimensional
3D – three-dimensional
Ala – alanine
App – adhesion and penetration protein
Arg – arginine
Asn, N – asparagine
Asp, D – aspartic acid
Å – Angstrom
BESSY – Berlin Electron Storage Ring Society for Synchrotron Radiation
Cryo-EM – cryo-electron microscopy
Cys, C – cysteine
DTT – dithiothreitol
E. coli – *Escherichia coli*
Frp – iron-regulated proteins
FrpC – iron-regulated protein FrpC
FrpD – iron-regulated protein FrpD
Fur – ferric uptake regulator
Gln – glutamine
Glu – glutamic acid
Gly, G – glycine
His – histidine
HSQC – heteronuclear single-quantum coherence spectrum
Hz – hertz
Ig – immunoglobulin
Ile, I – isoleucine
RTX – repeat in toxins proteins
Leu, L – leucine
Lys, K – lysine
MAD – multiwavelength anomalous dispersion
MIR – multiple isomorphous replacement
MR – molecular replacement
MspA – meningococcal serine protease A

M. smegmatis – *Mycobacterium smegmatis*
MW – molecular weight
NadA – *Neisseria* adhesin A
NCS – non-crystallographic symmetry
NhhA – *Neisseria* hia/hsf homologue A
N. meningitidis – *Neisseria meningitidis*
NMR – nuclear magnetic resonance
OD – optical density
Opa and Opc – opacity proteins
PBS – phophate buffered saline
PCR – polymerase chain reaction
PDB – protein data bank
Phe, F – phenylalanine
PPM – parts per million
SAD – singlewavelength anomalous dispersion
SAXS – small angle X-ray scattering
SeMet FrpD –selenomethionine-substituted FrpD
Ser – serine
SIR – single isomorphous replacement
SPM – self-processing module
TEV – tobacco-etch virus
Thr – threonine
T1SS – type I secretion system
TLS – translation/libration/screw groups
Tyr – tyrosine
Val – valine

1. Prologue and aims of thesis

Almost all aspects of life are engineered at the molecular level, and without understanding molecules we can only have a sketchy understanding of life itself.

Francis Crick (1988), *What Mad Pursuit: A Personal View of Scientific Discovery,* p. 61

1.1. Aims of the research

Neisseria meningitidis (*N. meningitidis*) is a Gram-negative commensal bacterium colonizing nasopharynx of about 10 % of healthy individuals. Occasionally, meningococci can penetrate into bloodstream and cause an invasive disease, such as life threatening sepsis, meningitis or other forms of meningocaccal pathologies causing morbidity (Cartwright *et al.,* 1987; Stephens, 1999; Tzeng & Stephens, 2000; Rosenstein *et al.*, 2001). Invasive behavior of *N. meningitidis* is thought to be correlated with production of two iron-regulated proteins (Frp), FrpC and FrpD (Thompson *et al.*, 1993; Osicka *et al*., 2001; Prochazkova *et al.*, 2005; Sviridova *et al.*, 2010).

Clinical isolates of *N. meningitidis* produce a repeat in toxin (RTX) protein FrpC. The FrpC protein belongs to the family of Type I-secreted RTX proteins, which are characterized by the presence of a variable number of nonapeptide RTX motif (L/I/F)XGGXG(D/N)DX (Thompson *et al.*, 1993; Osicka *et al.*, 2001; Osicka *et al.*, 2004). The biological activity of meningococcal FrpC protein remains unknown.

FrpD is a lipoprotein anchored to the *N. meningitidis* outer membrane. It is highly conserved among *N. meningitidis* strains and appears to be uniquely found in *N. meningitidis*. The primary amino acid sequence of FrpD does not exhibit significant similarity to any known proteins (Prochazkova *et al*., 2005; Sviridova *et al.*, 2010). The biological function of FrpD remains unknown. It is likely that the biological function of FrpD is associated with that of the FrpC protein, since FrpD was found to bind the N-terminal part of FrpC (residues 1-414) with very high affinity (K_D = 0.2 nM) (Prochazkova *et al*., 2005). The most probable function of the FrpD protein is participation in the anchoring of

the FrpC protein to the bacterial cell surface (Osicka *et al.*, 2001; Prochazkova *et al.*, 2005; Sviridova *et al.*, 2010).

Despite a few previous studies, our understanding of iron-regulated proteins of *N. meningitidis* remains shallow. Importantly, the molecular mechanism of function of Frp proteins remains unclear. Absence of structural data for the meningococcal Frp proteins is a huge barrier towards uncovering their mechanism of functional activity. In order to address this question we set out to determine the structure of the FrpD protein and its interaction mechanism with the FrpC protein.

We utilized the integrated structural biology approach in the present research. X-ray crystallography can provide very detailed atomic information, showing every atom in the protein along with atomic details of ligands, inhibitors, ions and other molecules that are incorporated into the crystal. However, it can only be applied provided diffraction-quality protein crystals are obtained. Therefore, it is advantageous to apply several methods for structural characterization of protein of unknown structure. Utilization of the integrated structural biology approach for structural characterization of the protein of interest is more effective than limiting yourself to a single technique.

The aim of this work was to perform explicit structural characterization of the iron-regulated protein FrpD protein from *N. meningitidis* and provide insights into its interaction mechanism with the FrpC protein.

The specific research objectives were to:

1. Determine the structure of the FrpD protein and analyze its folding
2. Determine the interaction interface between FrpD and FrpC proteins
3. Determine the structure of the FrpD-$FrpC_{1\text{-}414}$ complex
4. Provide insights into the structure-function relationship of FrpD and FrpC

2. Introduction

2.1. Characteristic of the *Neisseria meningitidis*

N. meningitidis is a Gram-negative diplococcus bacterium (Fig. 1). Meningococci are obligate commensals colonizing the nasopharyngeal mucosa of about 5 to 10 % of the humans without affecting the host. In most instances, *N. meningitidis* colonizes a human host without causing disease, a phenomenon known as carriage (Cartwright *et al.*, 1987; Virji, 1996; Stephens, 1999). The duration of the carrier state varies; it may be chronic, lasting for several months, intermittent or transient (Broome, 1986).

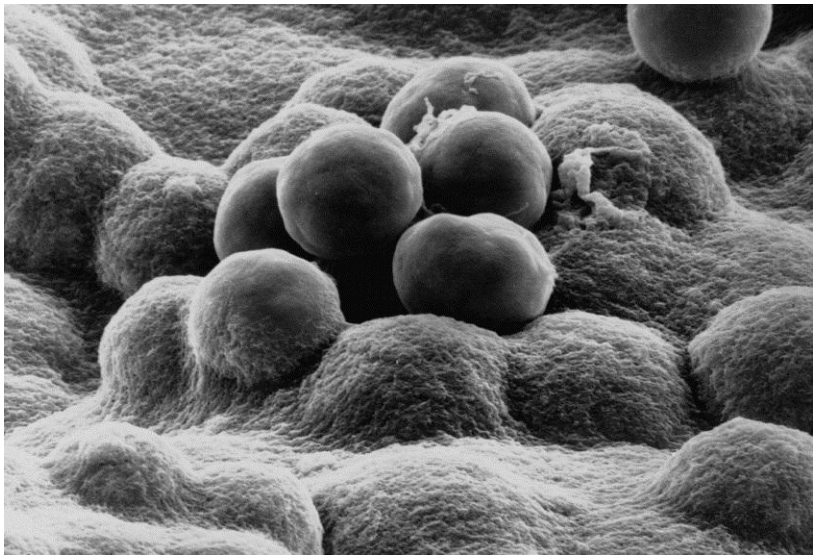

Figure 1. Scanning electron microscopy image of *N. meningitidis* (image courtesy of http://cmrf.research.uiowa.edu).

However, *N. meningitidis* occasional penetration of the mucosal membrane, invasion of the bloodstream and crossing the blood-brain barrier entails invasive meningococcal diseases such as meningococcal septicemia and/or meningitis (Anderson *et al*., 1998; Rosenstein *et al.*, 2001). Stephens and colleagues found that meningococci specifically bind nonciliated columnar epithelial cells (Fig. 2) (Stephens *et al*., 1983; Stephens, 2009).

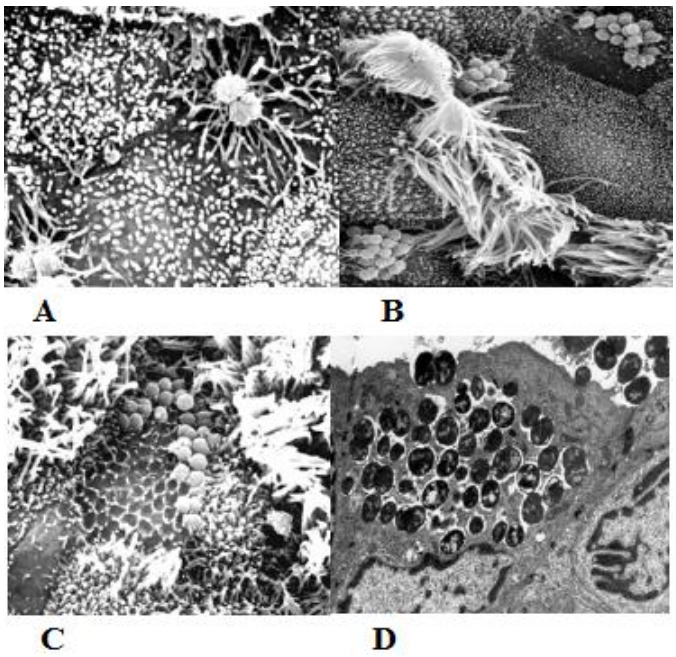

Figure 2. Events in carriage and invasion of *N. meningitidis*, (A) adhesion of the *N. meningitidis* to the epithelial cells, (B) microcolony formation, (C) cortical plaque formation and close adherence, (D) human epithelial cell invasion (Stephens, 2009).

There are 13 serogroups of *N. meningitidis* based on different capsular polysaccharide structures. However, only six serogroups (A, B, C, W-135, X, Y) cause most serious disease. Genome sequences for *N. meningitidis* strains MC58 (serogroup B), Z2491 (serogroup A) and FAM18 (serogroup C) have been reported (Tettelin *et al*., 2000). Serogroup A is responsible for epidemic outbreaks and predominates in Africa, whereas serogroups B and C prevail in industrialized countries and are associated with sporadic disease outbreaks (Virji, 1996). The persistence of serogroup A epidemic outbreaks in Africa, and the persistence of serogroups B and C disease in industrialized countries show that meningococcal infections remain one of the most serious medical emergencies worldwide (Hart and Rogers, 1993; Stephens *et al*., 2007).

Meningococcci can be encapsulated or unencapsulated, they elaborate adhesins, such as pili and outer-membrane opacity proteins, that may aid in anchorage to host mucosal cells, and specific nutrient acquisition factors (e.g. for the iron uptake). Encapsulation and secretion of immunoglobulin A (IgA)

protease, also aid in evasion of the host immune mechanisms (Virji, 1996; Hill *et al*., 2010).

N. meningitidis express a range of virulence factors including capsular polysaccharide, lipopolysaccharide (LPS) and surface-exposed adhesive proteins, which are essential for colonization of host tissues and bacterial survival on mucosal surface. Meningococcal virulence is induced by LPS which are the components of the outer membrane of *N. meningitidis*. LPS acts as endotoxin and is responsible for septic shock and hemorrhage due to destruction of host red blood cells (Stephens, 2009; Hill *et al*., 2010).

Adhesion of *N. meningitidis* to mucosal epithelia of human nasopharynx represents the first step of host colonization and consequent development of meningococcal pathogenesis. Adhesion to the host is a dynamic process resulting from a balance of interactions between the bacterial and host cell surface structures. Type IV pili are regarded as the major adhesins of *Neisseria* and rapid elongation of these polymeric filaments on the bacterial surface allows the initial attachment to the mucosal epithelia. Once the primary bacteria-cell contact is established, the pili are retracted and different repertoire of other adhesins orchestrates a deeper interaction with the host cell surface. Apart from the outer membrane opacity proteins (Opa and Opc), which promote the intimate adhesion and invasion of host cells, several minor adhesins, including *Neisseria* hia/hsf homologue A (NhhA), adhesion and penetration protein (App), *Neisseria* adhesin A (NadA) and meningococcal serine protease A (MspA), were shown to mediate binding to epithelial cells and facilitate bacterial colonization as well as spread (Capecchi *et al*., 2005; Mattick, 2002; Sadarangani *et al*., 2011; Scarselli *et al*., 2006).

2.2. Iron-regulated proteins of *N. meningitidis*

Acquisition of iron and iron complexes has long been recognized as an important determinant in the pathogenesis of *N. meningitidis* (Payne and Finkelstein, 1977). Iron starvation is used by many bacterial pathogens as a signal that they are in a host environment. In order for *N. meningitidis* to cause disease, it has to survive in various host environments, including the nasopharynx, oropharynx, bloodstream, and cerebrospinal fluid, which contain various forms and concentrations of free and complexed iron. The major source

of iron available to the meningococci is iron complexed to host iron-binding proteins. *N. meningitidis* has managed to overcome the iron limitation through the evolution of iron acquisition systems that rely on high-affinity receptors for iron-bound host proteins and enable it to use transferrin, lactoferrin, hemoglobin, and haptoglobin-hemoglobin as iron sources (Dyer *et al*., 1987; Mickelsen *et al*., 1981; Mickelsen *et al.* 1982; Schryvers and Stojiljkovic, 1999; Perkins-Balding *et al.*, 2004).

When bacterial pathogens are grown in iron-depleted conditions, similar to the conditions in host human body fluids, where the levels of free iron are extremely low, the expression of a number of virulence factors is increased (Grifantini *et al*., 2003). Transcriptional regulation in response to iron in Gram-negative bacteria is largely mediated by the ferric uptake regulator protein (Fur), which in the presence of iron binds to a specific sequence in the promoter regions of genes under its control and acts as a repressor (Hantke, 2001; Grifantini *et al*., 2004). As stated by Grifantini and colleagues, after iron addition to an iron-depleted bacterial culture of *N. meningitidis* group B (strain MC58), 80 genes were down-regulated and 153 genes were up-regulated, demonstrating that Fur can also act as a transcriptional activator (Grifantini *et al*., 2004).

The first reference to the iron-regulated proteins of *N. meningitidis* dates back to 1993, when Thompson discovered in meningococci two homologous secreted proteins, FrpC and FrpA that belong to the RTX family of proteins. The concept of RTX proteins characterized by the presence of arrays of glycine- and aspartate-rich nonapeptide repeats was first introduces by Welch in 1991.

RTX exoproteins are produced by a variety of Gram-negative bacteria with diverse biological functions and exhibit two common features. The first is the presence of a variable number of glycine- and aspartate-rich repeats, typically nonapeptides, binding Ca^{2+} ions. They are located in the carboxy-terminal portion of the protein and form numerous sites for the binding of Ca^{2+} ions (Welch, 1991; Welch, 2001; Linhartova *et al*., 2010). The second common feature is the unique mode of secretion of RTX proteins via the type I secretion system (T1SS). Protein translocation occurs through an oligomeric secretion channel spanning across the entire bacterial cell envelope including cytoplasmic

membrane, periplasmic space and outer membrane. Protein secretion via T1SS dedicated ATP-binding cassette transported-based secretion apparati recognize uncleavable C-terminal secretion signals and mediate single-step translocation of the RTX polypeptides from bacterial cytosol directly to the extracellular space. This process occurs without any periplasmic secretion intermediate (Linhartova *et al*., 2010).

At conditions of low iron availability (i.e. during meningococcal colonization of human nasopharynx and oropharynx), *N. meningitidis* secretes a family of FrpC-like, type I-secreted RTX proteins of unknown role in meningococcal lifestyle. Meningococci appear to carry a whole polymorphic family of *frpC*-like genes. Three of the iron-regulated *frp* (*frpA, frpC*, and *frpC*-like) alleles of *N. meningitidis* encoding proteins (FrpA, FrpC, and FrpC-like) were sequenced. FrpA is a 122-kDa protein that harbors 13 nonapeptide RTX repeats. FrpC is a 1829-residues long protein that harbors 43 copies of nonapeptide RTX motif (L/I/F)XGGXG(D/N)DX. FrpC-like protein is a 141-kDa protein encoded in the genome of the serogroup B isolate MC58 corresponding to the truncated version of the FrpC protein (Thompson *et al.*, 1993; Parkhill *et al*., 2000; Tettelin *et al*., 2000; Osicka *et al.*, 2001; Linhartova *et al*., 2010). Upon screening evaluation of 65 isolates of all serogroups of *N. meningitidis* the *frpA* allele was poorly conserved. In contrast, *frpC* alleles were detected in all invasive and most carrier strains of *N. meningitidis* (Osicka *et al.*, 2001).

Iron starvation also induces production of the FrpD protein, which is expressed from the gene located immediately upstream of the *frp*C gene in a predicted iron-regulated *frp*DC operon controlled by the Fur protein (Thompson *et al.*, 1993 a, b; Osicka *et al.*, 2001; Prochazkova *et al.*, 2005; Grifantini *et al*., 2003). The iron response in meningococci is mediated by the Fur protein that binds to a consensus promoter sequence (Fur-box) and transcriptionally regulates the expression of many virulence factors and iron-regulated genes. Of these, *frpD* and *frpC*, encoded consecutively in the *frpDC* operon, are overexpressed in *N. meningitidis* under iron-limited conditions (Fig. 3B) (Grifantini *et al*., 2003; Prochazkova *et al.*, 2005).

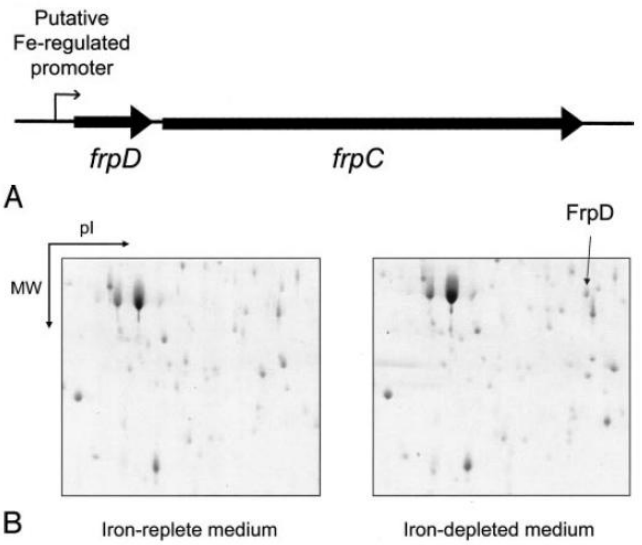

Figure 3. FrpD production is induced by iron-starvation. (A) Schematic representation of the predicted *frpD-frpC* operon of *N. meningitidis*, and (B) proteomic detection of iron-regulated expression of FrpD (Prochazkova *et al.*, 2005).

While the biological function of the Frp proteins remains unknown, the assignment of the Frp proteins to the RTX protein family suggests that they can play a role in meningococcal carriage and disease (Osicka *et al.*, 2001).

2.2.1. Iron-regulated protein FrpC

FrpC belongs to the family of RTX proteins, secreted through the T1SS and characterized by the presence of the C-terminal successive blocks of tandemly-repeated RTX nonapeptides with a consensus motif (L/I/F)XGGXG(D/N)DX (Osicka *et al.*, 2001; Osicka *et al.*, 2004). FrpC is a 1829-residues long protein with an amino-terminal portion of 876 residues and carboxy-terminal RTX moiety of 953 residues. The N-terminal segment of FrpC protein (residues 1-414) does not exhibit significant homology to any known protein sequence. (Thompson *et al.*, 1993, Osicka *et al.*, 2001, Osicka *et al.*, 2004). The C-terminal domain of the FrpC protein contains a large number of RTX repeats.

Osicka et al (2004) demonstrated that in presence of calcium ions the purified recombinant FrpC undergoes highly-specific processing that resembles

protein trans-splicing. This includes the Ca^{2+}-induced autocatalytic cleavage of the Asp_{414}-Pro_{415} peptide bond and subsequent covalent linkage of the released carboxyl group of Asp_{414} of the $FrpC_{1-414}$ fragment to an adjacent ε-amino group of another lysine residue through an isopeptide bond (Osicka *et al.*, 2004; Linhartova *et al.*, 2010). The *trans*-splicing activity of FrpC is mediated by a self-processing module (SPM), an adjacent segment of 177 residues (415–591) (Matyska Liskova *et al.*, 2016). The cleavage activity of SPM is closely associated with a Ca^{2+}-induced conformational switch of FrpC from an intrinsically unstructured to the folded state (Kuban *et al.*, 2015). SPM-mediated auto-processing of the FrpC protein is schematically represented in Figure 4.

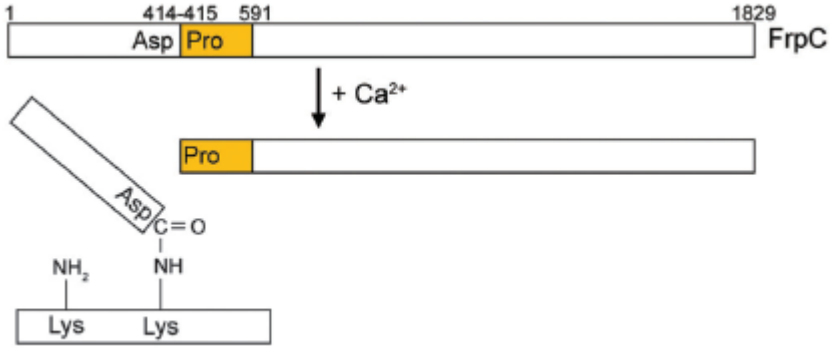

Figure 4. Schematic representation of calcium-dependent SPM-based splicing of FrpC protein. Binding of Ca^{2+} ions promotes the conformational change of the SPM that results in highly specific cleavage of the Asp414–Pro415 peptide bond and covalent linkage of the generated fragment ($FrpC_{1-414}$) to another protein molecule via newly-formed isopeptide Asp–Lys bond (Matyska Liskova *et al.*, 2016**)**.

The biological activity of meningococcal FrpC protein remains unknown. However, a number of RTX proteins were shown to be involved in virulence of Gram-negative bacteria (such as *Actinobacillus, Bordetella, Escherichia, Moraxella, Morganella, Pasteurella, Proteus,* and *Vibrio*) as exotoxins mostly exhibiting a cytotoxic pore-forming activity (Goebel & Hedgpeth, 1982; Muller *et al.*, 1983; Felmlee *et al.*, 1985; Welch, 1991; Osicka, *et al.*, 2004). High levels of both IgG and IgA class antibodies recognizing recombinant FrpC were detected in convalescent-phase sera of patients after meningococcal disease

(Osicka *et al.*, 2001). The elevated titers of antibodies against FrpC protein found in convalescent sera of patients from meningiciccal disease, suggest a poteintional role of FrpC protein in meningococcal carriage or virulence (Osicka *et al.*, 2001; Linhartova *et al*., 2010). However, FrpC was shown to be dispensable for virulence in the infant rat model of infection and its biological function remains unknown (Forman *et al*., 2003).

2.2.2. Iron-regulated protein FrpD

The protein investigated in the current research is a *N. meningitidis* iron-regulated lipoprotein FrpD. The first reference to this protein dates back to year 2005 when Prochazkova and colleagues first characterized FrpD protein as a unique lipoprotein embedded into the outer membrane of *N. meningitidis* (Prochazkova *et al*., 2005).

FrpD is an outer membrane lipoprotein, which is highly conserved in set of strains representative of all serogroups of *N. meningitidis* (Prochazkova *et al*., 2005). The primary amino acid sequence of FrpD does not exhibit significant similarity to any known proteins. The *frpD* gene sequence contains two translation initiation sites, which give rise to production of the full-length $FrpD_{271}$ (or $FrpD_{1-271}$) protein that harbours the N-terminal signal peptide promoting FrpD export across the cytoplasmic membrane by Sec translocase, and the truncated $FrpD_{250}$ (or $FrpD_{22-271)}$ protein that lacks the signal peptide and remains in cytoplasm of the bacteria. The exported $FrpD_{271}$ precursor is processed to its mature form on the periplasmic side of the cytoplasmic membrane, sequentially modified by a lipid molecule at Cys_{25} residue, and sorted to the outer bacterial membrane (Prochazkova *et al*., 2005; Kovacs-Simon *et al*., 2011). Both $FrpD_{271}$ ($FrpD_{1-271}$) and $FrpD_{250}$ ($FrpD_{22-271}$) isoforms bind the amino-proximal portion of FrpC with very high affinity (Prochazkova *et al.*, 2005; Sviridova *et al.*, 2010). Binding of FrpD does not preclude SPM-based splicing of FrpC (Prochazkova *et al*., 2005). The primary biological function of FrpD protein is still unknown. Poteintial functions of FrpD protein are likely related to anchoring to the bacterial cell surface and activity of the FrpC protein, since FrpD was found to bind the N-terminal part of FrpC (residues 1-414) with very high affinity K_D = 0.2 nM (Prochazkova *et al*., 2005).

FrpD most probably serves as an accessory lipoprotein that could be involved in anchoring of the secreted RTX protein FrpC protein to the outer bacterial membrane. However, the mechanism of FrpD-FrpC interaction is unknown due to the absence of structural information on both proteins.

2.3. Structural biology approaches

The structure of biological molecules is the key that reveals their function. The aim of structural biology is to deduce how biological molecules function by determining the three-dimensional (3D) arrangement of their atoms. There are a number of different techniques for determination of protein structure such as: X-ray crystallography, nuclear magnetic resonance (NMR) spectroscopy, cryo-electron microscopy (Cryo-EM) and small-angle X-ray scattering (SAXS) (Chasman, 2003; Rhodes, 2006; Rupp, 2010).

By the present time more than 100 000 structures of biomolecules have been deposited to the Protein Data Bank (PDB). Around 90% of the deposited into PDB structures were determined by X-ray crystallography; about 10% of structures were derived from NMR spectroscopy and some structures are determined by Cryo-EM (www.pdb.org).

Structural biologists use different methods to study structure-function relationships of proteins and protein complexes. Since structural studies generally only provide snapshots of molecules, the integration of structural data derived using different technologies is crucial to understand, on the basis of the detailed atomic structure, how proteins, protein complexes or whole pathogens interact dynamically with their functional environment (Lander *et al*., 2012).

2.3.1. X-ray crystallography

X-ray crystallography is a technique used for identifying the atomic and molecular structure of a crystal, in which the crystalline atoms cause the beam of incident X-rays to diffract into many specific directions. Provided that the molecule or complex of interest can be crystallized, X-ray crystallography yields atomic resolution and is not limited by the size of the molecule. By measuring the angles and intensities of these diffracted beams crystallographers can produce a 3D picture of the density of electrons within the crystal. From

this electron density, the mean positions of the atoms in the crystal can be determined, as well as their chemical bonds, their disorder and various other parameters (Drenth, 1994; Rhodes, 2006; Rupp, 2010).

Determination of the 3D structure of molecules using X-ray crystallography consists of several steps. The molecule of interest (e.g. protein) should be purified, crystallized and the diffraction-quality protein crystal should be subjected to an intense beam of X-rays. It is mandatory to use X-rays for the diffraction data collection because the atoms in the molecule are separated by distances in the range of angstroms (Å). The collected diffraction images should be processed and the phase problem should be solved in order to produce an electron density map. A model of the structure that is built based on the electron density map should be refined, validated and deposited to the PDB (Drenth, 1994; Rupp, 2010).

2.3.1.1. Protein crystallization

The process of crystallization molecules of any compound (including proteins) from its solution represents a reversible equilibrium phenomenon, driven by the minimization of the free energy of the system (Weber, 1991). A protein will stay in solution only up to a certain concentration. Once this limiting concentration is reached, the solution will no longer remain homogeneous, but a new state or phase will appear. This phenomenon forms the basis of all protein crystallization experiments. The main principle of crystallization is to bring the system into a state of limited degree of supersaturation by modifying the properties of the solvent through equilibration with a precipitating agent (such as polyethylene glycol, ammonium sulfate etc.), or by altering some physical properties (such as temperature, vibrations, time, pressure etc.) (McPherson, 1999; Asherie, 2004).

Protein crystallization absolutely requires the creation of the supersaturated state. This is a non-equilibrium condition in which there is number of the protein molecules, which exceed the solubility limit, under specific chemical and physical conditions, are nonetheless present in solution. Equilibrium is re-established by formation and development of a solid state, such a crystals, as the saturation limit is attained.

Protein crystallization proceeds in three stages: nucleation, growth, and cessation of growth. Nucleation represents a first order phase transition by which molecules pass from a completely disordered state to an ordered one. During nucleation enough molecules associate in three dimensions to form a thermodynamically stable aggregate "critical nucleus" (McPherson, 2004). A process of crystal nuclei formation and growth can be described by the two-dimensional (2D) solubility diagram shown below (Fig. 5).

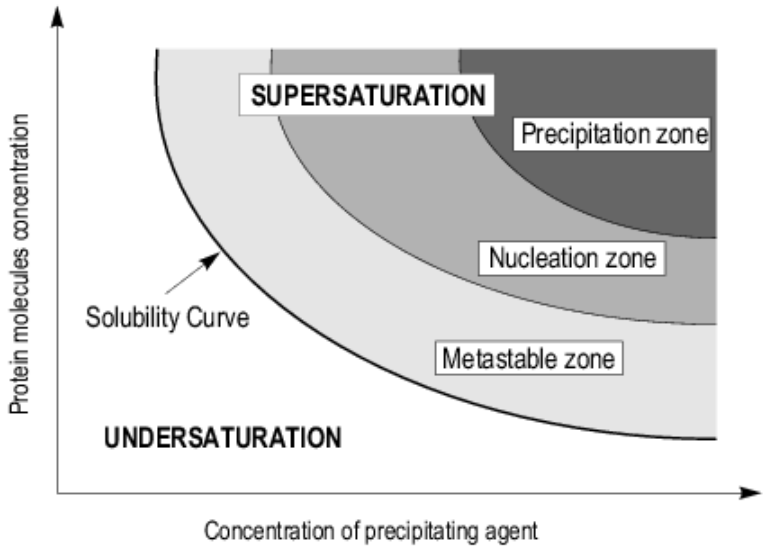

Figure 5. Crystallization phase diagram, illustrating the change of protein molecules concentration against precipitating agent concentration (Ducruix & Giege, 1992).

The solubility curve divides the concentration space into undersaturated and supersaturated zones. The solubility curve corresponds to a concentration at which the solution is in equilibrium with the precipitant. In the area under the solubility curve, the solution is undersaturated and the crystallization will never take place. Above the solubility curve lays the supersaturation zone. At the supersaturation zone, for a given concentration of precipitant, the protein concentration is higher than that at equilibrium. The supersaturation zone may be subdivided into: precipitation zone (where the excess of protein molecules immediately separates from the solution to form amorphous aggregates), nucleation zone (where the excess of protein molecules aggregates in a

crystalline form) and metastable zone (a supersaturated solution may not nucleate for a long period, unless the solution is mechanically shocked or a seed crystal introduced) (Ducruix & Giege, 1992).

Growth of protein crystals is a better characterized process than nucleation. Protein crystals grow by the classical mechanisms of dislocation growth and 2D nucleation, along with two other less common mechanisms known as normal growth and 3D nucleation (Malkin *et al*., 1995; McPherson *et al*., 2003). Crystal growth ceases when the solution is sufficiently depleted of protein molecules, deformation-induced strain destabilizes the lattice, or the growing crystal faces become poisoned by impurities.

Protein crystals are composed of approximately 50 % solvent on average, through this may vary from 25 to 90 % depending on the particular macromolecule. Protein molecules occupy the remaining volume of the crystal (McPherson, 2004). Protein crystals of different shapes are demonstrated in Figure 6.

Protein crystals grow from aqueous solutions, ones to which they are tolerant. These solutions are called mother liquors. Protein crystals are limited in size, are very soft and crush easily, disintegrate if allowed to dehydrate, exhibit weak optical properties, and poorly diffract X-rays (McPherson, 2004). Protein crystals are temperature sensitive and undergo extensive damage after prolonged exposure to radiation. Therefore, frequently several crystals must be analyzed for a structure determination to be successful (Garman, 2010).

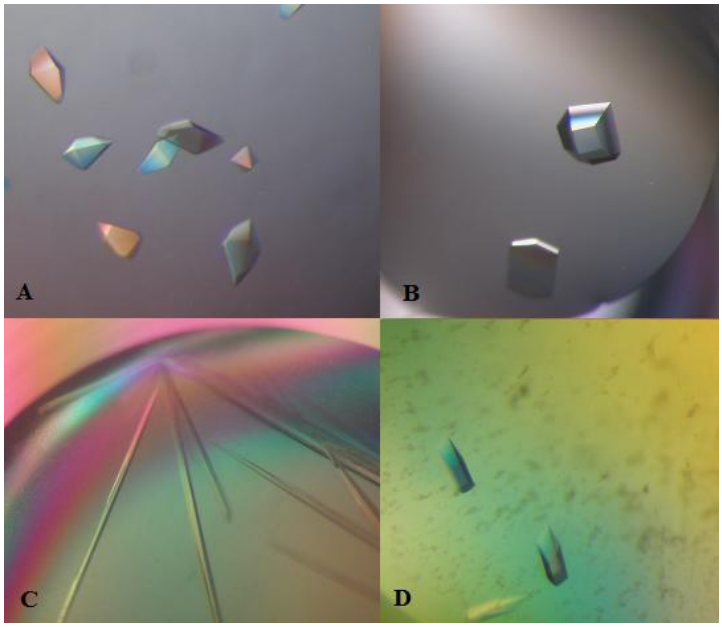

Figure 6. Protein crystals of different shape: (A) histidine phoshotranser protein 2 AHP2 from *Arabidopsis thaliana*, (B) lysozyme from hen egg white, (C) mutant haloalkane dehalogenase LinB from *Sphingobium japonicum*, and (D) BopN an effector protein from *Bordetella pertussis.*

2.3.1.2. Crystallization techniques

A number of techniques for setting up crystallization experiments have been developed. Among them, the following methods are frequently used: vapor diffusion (sitting, hanging and sandwich drop), batch and microbatch under oil, dialysis, and counter-diffusion (free interface) diffusion (Ducruix & Giege, 1992; McPherson, 1999; Chayen, 1999).

The choice of method depends on the protein involved, its quantity and on the preference of the experimenter. Vapor diffusion and batch are the most widely used techniques due to the relative ease of their implementation in comparison with the other methods. Automatic systems have been developed for both vapor diffusion and batch techniques (Chayen, 1999).

Vapor diffusion is the optimal techniques when screening a large number of conditions. Typically, a small droplet of the protein solution is mixed with a droplet of the precipitant solution. The drop is then suspended or not (up to choice of the experimenter) and sealed over the well solution. In hanging drop

method the drop is placed on a cover slide, which is flipped and sealed over the reservoir containing the precipitant solution (Fig. 7A). Sitting drop method utilizes the same principle as hanging drop, except that the drop is placed on a concave sitting drop post and the system is isolated by a transparent sealing tape (Fig. 7A). The volume of the hanging drop is limited to about 8-10 µl, since bigger volumes might cause the drop to fall out of the cover slip. This limitation is eliminated in the sitting drop technique. In sandwich drop, the sample solution mixed with the precipitant is placed in the middle of a lower cover slide and covered with a larger cover slide in position along an upper edge, in such a way that the drop is sandwiched between the cover slides (Fig. 7A) (Chayen, 1992; Bergfors, 1999).

Equilibration proceeds by diffusion of water or organic solvent until vapor pressure in the drop equals that of the reservoir. This process leads to the change of the concentration of all constituents in the drop. During a vapor diffusion experiment, the protein will start to concentrate from an unsaturated state to reach a supersaturated state. As the first crystals appear the concentration of the protein will decrease. The crystals will then grow until the concentration of the protein in the drop reaches the solubility curve (Chayen, 1992; Bergfors, 1999).

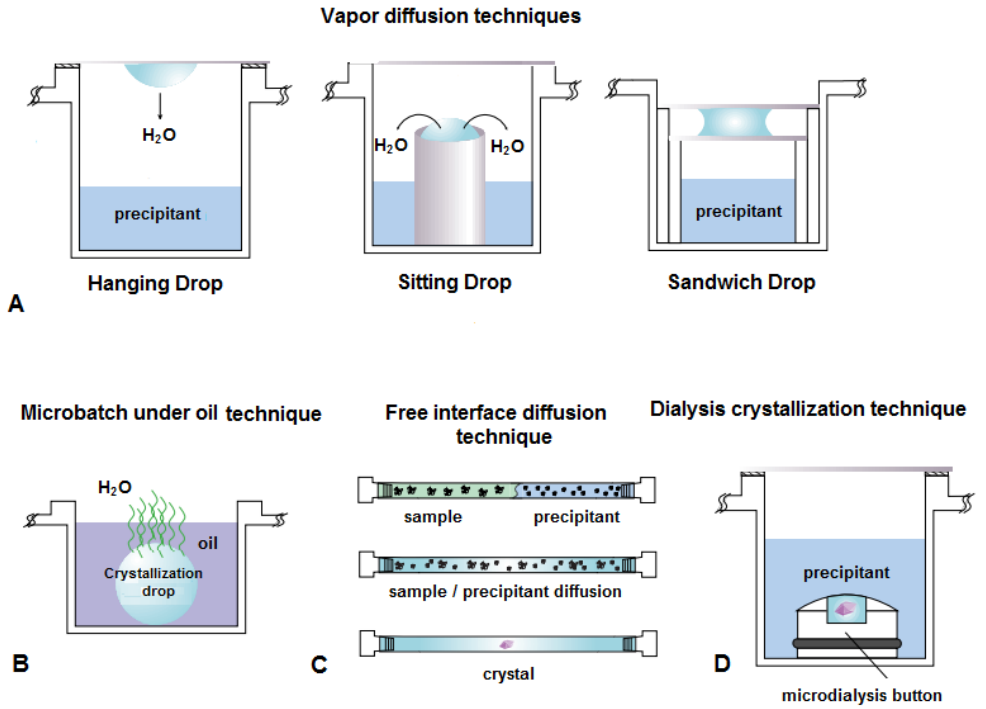

Figure 7. Schematic representation of protein crystallization techniques. (A**)** vapor diffusion (hanging, sitting and sandwich drop), (B) microbatch crystallization, (C) free interface diffusion, and (D) dialysis crystallization (modified from https://hamptonresearch.com).

Batch crystallization is a method where the molecule to be crystallized is mixed with the crystallization agent in a Petri dish at the required concentration at the start of the experiment. Supersaturation is thus achieved immediately upon mixing. A modification of the batch technique is microbatch under oil, where a small drop of the sample is mixed with the precipitant agent and placed under a layer of mineral oil (Fig. 7B) (Chayen, 1992; Bergfors, 1999).

Counter-diffusion (free interface diffusion) is the method where equilibration proceeds by the diffusion of two solutions placed in a glass capillary, which creates a concentration gradient (Fig. 7C). One solution contains the protein sample and the other solution contains the crystallizing agent. Two solutions are set to diffuse against each other, resulting in a gradient supersaturation along the length of the capillary. The gradient increases the probability to reach supersaturation where the well ordered single crystals will grow (Garcia-Ruiz, 1991; Garcia-Ruiz, 2003).

Dialysis techniques utilize diffusion and equilibration of small precipitant molecules through a semipermeable membrane as a means of slowly approaching the concentration at which the macromolecule solute crystallizes. Initially, the protein solution is contained within the dialysis membrane, which is then equilibrated against a precipitant solution (Fig. 7D). Equilibration proceeds by diffusion of small molecules (ions, additives, buffers) through a semipermeable membrane into the sample compartment. Equilibration against the precipitant in the surrounding solvent slowly achieves supersaturation for the solute within the dialysis membrane, eventually resulting in crystallization. The advantage of the dialysis is that the precipitating solution can be easily changed. Thus, the protein solution can be continuously recycled until the correct conditions for crystallization are found (Weber, 1997).

2.3.1.3. Crystal geometry and symmetry

Crystal is an orderly 3D array of molecules, held together by noncovalent interactions, in which atoms are arranged in a crystal lattice constructed of identical unit cells. Unit cell is the smallest portion of the complete space lattice which, when repeated over and over again in different directions, produced the complete space lattice. Each crystal consists of planes of atoms that are spaced at a distance *d* apart.The unit cell is defined with dimensions *a*, *b*, and *c* and three angles α, β and γ between them. The asymmetric unit is the smallest unit of the structure that can generate the whole crystal after application of the crystal symmetry (Fig. 8). Knowing the space group, the unit cell, and the contents of the asymmetric unit one can define the positions of all atoms in the crystal (Rhodes, 2006).

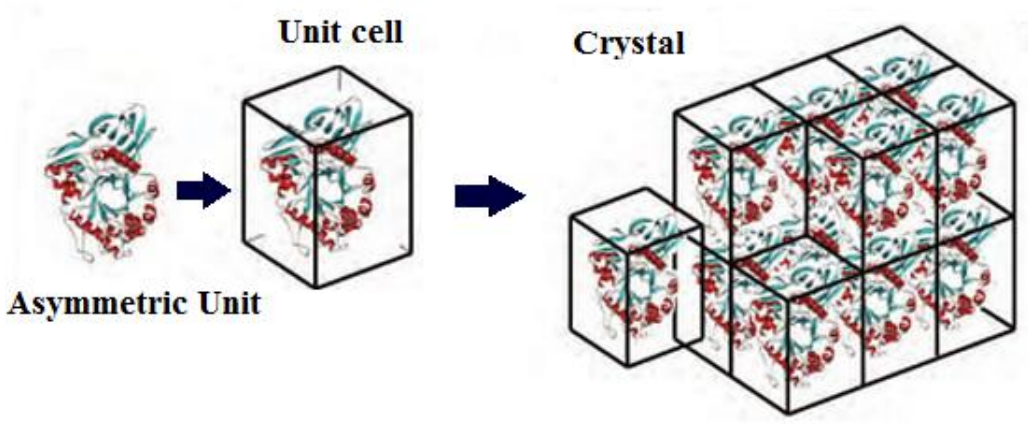

Figure 8. Assembly of a primitive triclinic crystal from unit cells (modified from Rupp, 2010).

Symmetry is a set of operations, the application of which superimposes the structure on itself so that it is indistinguishable from the original. There are three different types of symmetry evident in the shape of crystals: rotation, reflection and inversion. Reflection and inversion symmetries can only occur when the molecule in the crystal exists in both chiral forms. Since proteins are single-chirality molecules, they are restricted to build lattices that only contain rotational symmetry (McPherson, 1999). Only 2-fold (180°), 3-fold (120°), 4-fold (90°) and 6-fold (60°) rotation symmetries are allowed. The elements of symmetry in the unit cell define the so called space group of the crystal. On the basis of the shapes for the unit cell parallelepipeds the space groups belong to seven crystal systems (triclinic, monoclinic, orthorhombic, trigonal, tetragonal, hexagonal and cubic). When combining with the lattice centering operations (P, R, I, F, A, B, C), the 7 crystal systems give 14 distinct lattices, called Bravais lattices (Lockwood and Macmillan, 1978).

The lattice of the crystals can be enantiomorphic even if the molecules within have only one chirality. Screw rotations are written using the order of the rotation (2, 3, 4 or 6) followed by a subscript indicating the fraction of the unit cell of the translation. For example 2_1 is a 180° rotation with ½ unit cell translation. There are 11 crystallographically allowed screw rotation symmetries (2_1, 3_1, 3_2, 4_1, 4_2, 4_3, 6_1, 6_2, 6_3, 6_4, 6_5). Screw rotations are important biologically because they enable chains of molecules to link together.

Combining all crystallographic point groups and lattice types produces a total of 230 unique space group symmetries. Of the 230 crystallographic space groups, only 65 space groups re possible for chiral molecules such as proteins, DNA and RNA (McRee, 1999; Hahn, 2002).

2.3.1.4. X-ray data collection and data processing

In order to produce significant diffraction, the spacing between the scatterers and the wavelength of the impinging wave should be similar in size. One can use an X-ray diffractometer for collection of the diffraction data from large crystals, but for crystals with dimensions of the order of 100 nm or less it is necessary to use a synchrotron source (Fig. 9A) (Rhodes, 2006).

First, it is nessesary to collect all the reflections from the crystal (Fig. 9B). Practically, a crystal is mounted in a small loop or capillary tube between an X-ray source and an X-ray detector and flash-cooled in a 100 K liquid nitrogen stream. In order to increase the quality of X-ray data collection cryoprotectants (such as glycerol, xylitol, glucose, polyethylene glycol, and/or high salt concentrations) are used for suppression of the crystalline ice formation by flash-freezing crystals (Garman, 1999; Rubinson *et al*., 2000). The crystal lies in the path of a narrow beam of X-rays coming from the source. Collection of all reflections from the crystal requires that the crystal is rotated with respect to the incoming X-ray beam through 180°. Each diffraction image is recorded with the crystal rotated usually through a small angle of between 0.1° and 1°. Each diffraction image thus represents a wedge of data. Resolution defines the amount of the detail that can be seen in the experimental data. The quality of the collected data mostly depends on the quality of the crystals and their crystalline order. The more ordered crystals will diffract to a higher resolution (Drenth, 1994; Rhodes, 2006; Rupp, 2010).

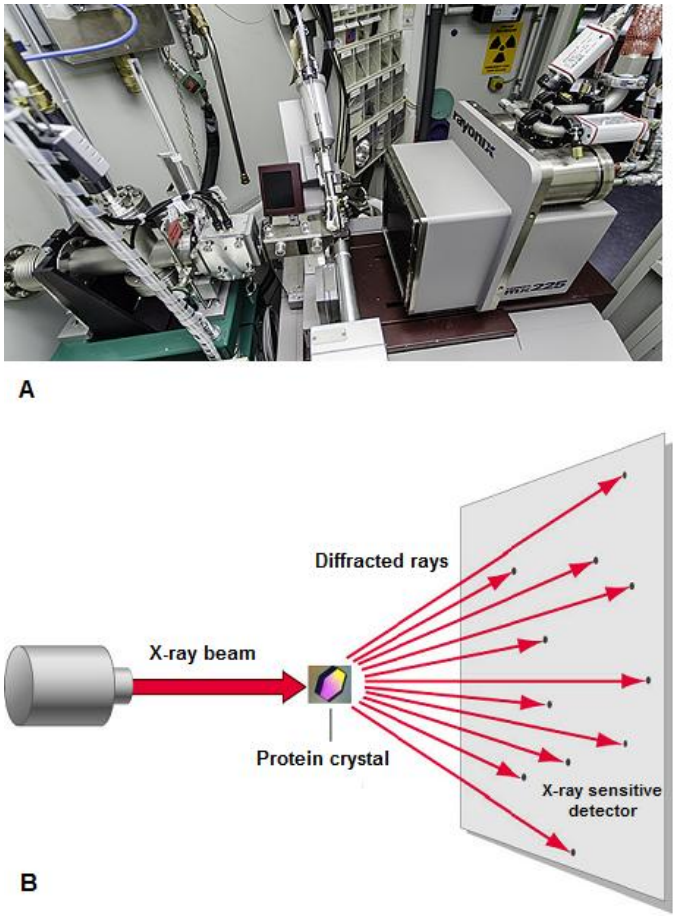

Figure 9. Representations of: (A) a synchrotron beamline station setup (image courtesy of https://www.helmholtz-berlin.de), and (B) the overall scheme of X-ray diffraction experiment.

After the data collection, a data set of a large number of diffraction images should be analyzed. Data processing begins with scanning the image to find regions that have spots of intensity higher than the background. Then the positions of the reflections are analyzed in order to define the unit cell parameters. Each reflection obtained after the data collection is assigned three coordinates in the imaginary 3D space of the diffraction pattern (reciprocal space). These indices *h*, *k*, and *l* are called Miller indices (Rhodes, 2006).

2.3.1.5. X-ray diffraction by crystals and the phase problem

X-rays can be described as an electromagnetic wave that interacts with the electon cloud that surrounds the atoms in the crystal. When electrons get hit by X-rays they emit radiation. The radiation emitted by the whole crystal is the summation of waves each scattered by one electron. The diffraction occurs if the scattered waves interfere with each other and those being in phase are added together and contribute to a system of symmetrically arranged spots (reflections) forming a diffraction pattern on the detector. This phenomenon is described by the Bragg's law:

$$2d \sin \theta = n\lambda$$

where d is the distance between atomic layers in the crystal, θ is the angle of incidence of the X-ray beam, n is a positive integer, and λ is the wavelength of the incident X-ray beam (Rupp, 2010).

The position of a reflection is related to the angle by which the diffracted beam diverges from the source beam. The reflections can be characterized by a structure factor. Structure factor $F(hkl)$ is a complex number that represents the total scattering from all atoms of the unit cell and includes structure factor amplitude $|F(hkl)|$ and relative phase angle $\varphi(hkl)$ between the diffracted waves. Calculation of the electron density function $p(xyz)$ allows to obtain an electron density map (distribution of electrons in space), which allows to define the coordinates of atoms in the molecule. The relationship between the structure factor $F(hkl)$ and the electron density function $p(xyz)$ can be expressed through the Fourier transformation, where the structure factors $F(hkl)$ containing the information about amplitudes $|F(hkl)|$ and phases $\varphi(hkl)$ are used as Fourier coefficients to generate the electron density map of the protein (Rhodes, 2006; Rupp, 2010):

$$\rho(xyz) = \frac{1}{V} \sum_{\substack{hkl \\ -\infty}}^{+\infty} |F(hkl)| \, . \, e^{-2\pi i[hx+ky+lz-\phi(hkl)]}$$

Many different detector technologies have been used for recording the intensities of the reflections. However, for each reflection on the diffraction pattern it is only possible to measure the intensity of the diffracted wave. Therefore, the diffraction patterns are the measured intensities of the structure factors that are proportional to the square of the amplitudes of the structure factors:

$$I(hkl) \propto |F(hkl)|^2$$

Since the phase information of the structure factors cannot be measured this fact is known as the phase problem (Drenth, 1994; Grune, 2005; Rupp, 2010).

2.3.1.6. Solving the phase problem

There are three main strategies for solving the phase problem: direct methods, molecular replacement and experimental phasing (Grune, 2005).

Direct methods allow deriving phases from the intensity of the reflections alone. Direct methods are statistical methods that use probabilistic relationships between the phases (Sayre, 1952). However, they can be used only if the data are of a very high resolution (better than 1.2 Å) and there are less than 200 non-hydrogen atoms in the structure. Therefore, except for peptides and the smallest proteins, direct methods cannot be used to solve protein structures (Taylor, 2003).

Molecular replacement (MR). Non-crystallographic symmetry (NCS) exists when more than one identical object is present in the asymmetric unit (Rupp, 2010). The first utilization of NCS as a tool for structure determination was introduced by Rossmann and Blow (Rossmann & Blow, 1962). The term "molecular replacement" was introduced in the name of a book in which the early papers were collected and briefly reviewed (Rossmann, 1972). MR allows obtaining phases from the already known structure of protein, which is similar to the unknown protein of interest based on sequence identity. The sequence identity should be better than 25 % and a root mean square deviation between C^{α} atoms of the model and the target should be less than 2.0 Å. This assumes

that there are no conformational differences between the two structures (Taylor, 2003).

The information contained in the known structure has to be transferred to the unknown crystal structure of the protein of interest. That means that a proper orientation and the proper translation have to be found. For doing that Patterson methods are usually used (Taylor, 2003; Evans and McCoy, 2007). MR can be carried out using different programs such as Phaser, Molrep, MrBump, etc. Most of these programs use a procedure in which first a rotation function search is performed, followed by a translation function search. The MR is an extremely fast method for solving the phase problem, provided that a good model structure is available (Scapin, 2013).

There are several methods for **experimental phasing** such as: single and multiple isomorphous replacement (SIR and MIR), single and multiwavelength anomalous dispersion (SAD and MAD), and combination of single and multiwavelength isomorphous replacement with anomalous scattering (SIRAS and MIRAS). All these techniques require a heavy atom to be present in enough sites in the molecule to give a clear signal. There are several classes of heavy-atom derivatives available for phasing that can be can be incorporated into the protein (e. g. selenomethionine derivatives or metal-containing proteins), or soaked into the crystal (heavy atoms, halogens, halides, etc.) (Garman and Murray, 2003).

Isomorphous replacement (SIR and MIR). The presence of heavy atoms in crystals is used to get the initial phases. M. Perutz and J. Kendrew first applied this method to proteins (Kendrew *et al*., 1958). They used soaking of the protein crystals in heavy-atom solutions in order to create isomorphous heavy-atom derivative crystals, which have the same unit cell and the same orientation of the protein in the unit cell. Creation of the isomorphous heavy-atom derivative crystals is also possible using co-crystallization with the heavy atoms. The differences between the native and derivative crystals, which gave rise to measurable intensity differences, are used to deduce the positions of the heavy atoms in the crystal. The structure factor equation of the derivatives can be written as:

$$F_{PH} = F_P + F_H$$

where F_P is the structure factor of the native protein and F_H is the contribution of the heavy atom (Blow & Crick, 1959; Drenth, 1994; Read, 2003).

Practically, intensities of native crystals and one (SIR) or more than one (MIR) derivatives are collected. The difference between the derivative and native structure factors are used for phasing. Phase determination with SIR leads to two possible solutions (two-fold phase ambiguity). Unambiquous phase determination can be achieved using MIR. The major problem of isomorphour replacement technique is the creation of the perfectly isomorphous derivative crystals (Taylor, 2003; Garman and Murray, 2003).

Anomalous dispersion (SAD and MAD). In anomalous dispersion experiments, the phases are derived using the differences in structure factor amplitudes arising from anomalous scattering of particular atoms present in the crystal. Crystallographers use the method of adding a few strongly anomalously scattering atoms that can be incorporated into the protein, or soaked into the crystal. The contribution of these atoms to the diffraction data is strong and using the positions of these atoms in the crystals, one can get the positions of the rest of the diffracting atoms of proteins in the crystal (Taylor, 2003; Grune, 2005).

Anomalous scattering properties of elements occur at specific wavelengths, which are close to the absorption edge of the element. When the frequency of the X-rays is near the absorption edge of the element, an electron is ejected from the core of the atom and a photon can be absorbed (Taylor, 2003).

The atomic scattering factor of an anomalous scatterer can be described as:

$$f_{ano} = f_0 + f'(\lambda) + if''(\lambda)$$

where f_0 is the normal scattering factor contribution, f' is the dispersive signal and f'' is the anomalous signal. Friedel's Law states that the structure factor amplitudes (or measured intensities) of reflection with conjugate phase are identical. If the crystal contains "anomalously" scattering atom this leads to

breakdown in the Friedel's law: $|F(hkl)| \neq |F\text{-}(hkl)|$, giving rise to anomalous differences that can be used to locate the anomalous scatterers (Taylor, 2003).

In case of a SAD experiment just one data set is collected at the wavelength corresponding to the absorption peak of the element (Dodson, 2003). During the MAD experiment the data is collected at several wavelengths (typically three), in order to maximize the absorbtion and dispersion effects. Typically, wavelengths are chosen at the absorbtion peak of the element, at the point of inflection on the absorption curve, and at a remote wavelength, because on these points the anomalous scattering factors are significantly different from each other (Ogata, 1998; Garman and Murray, 2003).

2.3.1.7. Model building, refinement and validation

Once the phases are obtained and the electron density function is calculated, the graph of this function is used to produce an electron density map. The electon density map has to be interpreted by building a model that fits it. Special computer programs are used for the interpretation of all crystallographic data. During the intepritation of the electron density map and building the model, all current knowledge about the protein under investigation (especially, the information about the sequence of amino acids in the protein) have to be used. The final model must be consistent with the experimental data and must be chemically realistic. It means that the model must possess bond lengths, bond angles, conformational angles, and distances between neighboring groups that are all consistent with the established principles of stereochemistry (Drenth, 1994; Rhodes, 2006; Rupp, 2010).

The phases obtained experimentally or by MR can be improved using different density modification techniques such as solvent flattening (Wang, 1985), histogram matching (Zang *et al*., 2001), NCS averaging (Vellieux *et al*., 1997), maximum-likelihood density modification (Terwilliger, 2000) and sphere of influence method (Sheldrick, 2002). Density modification approaches use some conserved features of correct electron density maps to improve the observed map. Generally, it is carried out in a two steps. First the electron density map obtained experimentally is modified in real space in such a way that it is consistent with the expectations. Then phases are calculated from this

modified map and combined with the experimental phases to form a new set of phases (Rhodes, 2006; Rupp, 2010).

The model obtained after density modifications usually is not very accurate and incomplete. These issues can be fixed using iterative model building via inspection of the electron density map and cycles of structure refinement. Each crystallographic model is described by the atomic coordinates and by the atomic displacement parameters. During the structure refinement, depending on the resolution and on the data-to-parameter ratio, the structure can be modeled as isotropic, anisotropic or using translation/libration/screw (TLS) groups (Painter & Merritt, 2006). The data-to-parameter ratio can be artificially increased using constraints or restraints. The constraints are exact mathematical conditions that decrease the number of parameters while the restraints are additional observational equations that increase the amount of data (Rupp, 2010).

There are two approaches that are used in the refinement of macromolecules: least-squares and maximum likelihood. In least-squares method the observations (experimental intensities) have fixed values and the parameters are varied in such a way that the calculated values approach the observed ones as closely as possible. The program SHELXL utilizes the least squares method (Sheldrick *et al*., 1997). This kind of refinement works well only for models for which high resolution data are available. The program REFMAC (Murshudov *et al*., 1997) utilizes the maximum-likelihood approach, which involves giving the model the probability function (likelihood function) (Pannu *et al*., 1996).

There are two important criteria of the accuracy of a structure refinement: the crystallographic R factor and its cross-validation equivalent, R_{free}. The R factor determines how well the atomic model is supported by the experimental data found in the structure factor file. R_{free} is used to avoid overfitting. For the calculation of R_{free} a small percentage of the data (around 5 %) are not used in refinement and their agreement with the refined data is monitored (Brunger, 1992; Kleywegt, 2000).

After refinement the model should be validated using local geometry validation programs such as: PROCHECK (Laskowski *et al*., 1993), WHATCHECK (Hooft *et al*., 1996), MolProbity (Chen *et al*., 2010). Local

geometry validation programs evaluate the model geometry on per-residue basis and flag outliers. To fix model errors, the density around the questionable residues should be inspected, necessary corrections should be made and then the corrected structure should be refined again (Rupp, 2010).

When the crystal structure is solved and validated, the contents of the asymmetric unit that has been modeled must be deposited and made available through the PDB. The PDB archive contains two types of data for crystal structures. The coordinate files include atomic positions for the final model of the structure, and the data files include the structure factors from the structure determination (Rhodes, 2006).

2.3.2. NMR spectroscopy

NMR spectroscopy is a powerfull tool for high-resolution structural characterization of protein molecules in solution. Models of proteins in solution can be derived from NMR spectroscopy. Moreover, NMR spectroscopy is a useful method for studies of kinetic reactions and properties of proteins at the atomic level. However, the atomic structure determination using NMR is restricted to molecules or complexes with molecular weights (MW) below 40–50 kDa (Bax, 1994; Keeler, 2005; Kwan *et al*., 2011).

NMR uses the property of atomic nuclei with odd numbers of protons and neutrons (such as ^{1}H, ^{13}C, ^{15}N, ^{31}P, etc.) to have a spin, which means they rotate around a given axis. The nucleus with a spin is a charged and spinning particle, which adopts preferred orientations in the magnetic field. The magnetic field developed by the rotating nucleus is described by a nuclear magnetic moment vector. The orientations of nuclear spins can be altered by pulses of electromagnetic radiation in the radio-frequency range (Rhodes, 2006).

Nuclei in different chemical environments absorb different frequencies of energy. This allows specific nuclei to be detected by their specific absorption energy. This energy, which can be expressed in hertz (Hz), depends on the strength of the magnetic field. Therefore, it is expressed as a frequency difference between that of the nucleus under investigation and a standard nucleus (e.g. hydrogen in tetramethylsilane) divided by the strength of the magnetic field. The result is called a chemical shift. The chemical shift is usually expressed in parts per million (ppm). The chemical shifts in proteins

depend strongly on local chemical structure and the structural geometry of the protein molecules (Rhodes, 2006; Shen *et al*., 2009).

Nuclear spins interact magnetically, exchanging energy with each other by a process called spin-spin coupling. Spin-spin coupling distributes or splits the absorption signals of nuclei about their characteristic absorption frequency. Spin-spin coupling can be used for determination of nuclei located next to each other in the molecule of the investigation (Rhodes, 2006).

One of the most useful and sensitive NMR spectra is the one-dimensional ^{1}H-NMR spectrum, which simply shows signals for each of the hydrogen atoms in the molecule under investigation. The other useful NMR spectrum is the 2D ^{15}N-labeled heteronuclear single-quantum coherence (HSQC) spectrum, which shows signals for each covalently bonded ^{1}H-^{15}N group. Each signal in the 2D ^{15}N-HSQC spectrum has an intensity and two chemical shifts (one for ^{1}H and second for ^{15}N nucleus). ^{15}N-HSQC spectrum of good quality should contain one peak for each amide proton (e.g. for each peptide bond, except those preceding prolines), a peak for each indole -NH or tryptophan residues, and pairs of peaks for the sidechain amide groups of each Asn and Gln residue. Signals from the guanidine groups of arginine can also be observed. The ^{15}N-HSQC spectrum should contain one peak for each residue in the protein (Kwan *et al*., 2011).

It is often a great advantage for the NMR spectroscopy to introduce the NMR active stable isotopes ^{13}C and ^{15}N in the protein of interest. With the introduction of ^{13}C and ^{15}N nuclei the spins in a protein are almost all being connected by one-bond couplings. The preparation of proteins enriched with these two nuclei are accomplished by the expression of the protein of interest in microorganisms grown in minimal growth medium where the carbon source is fully ^{13}C labeled and the nitrogen source is fully ^{15}N labeled (Poulsen, 2002).

Analysis of multidimensional NMR spectra leads to three primary sets of structural restraints (interproton distances, dihedral angles and hydrogen bonds) that are used to a computer algorithm to reconstruct the model of the molecule (Fig. 10).

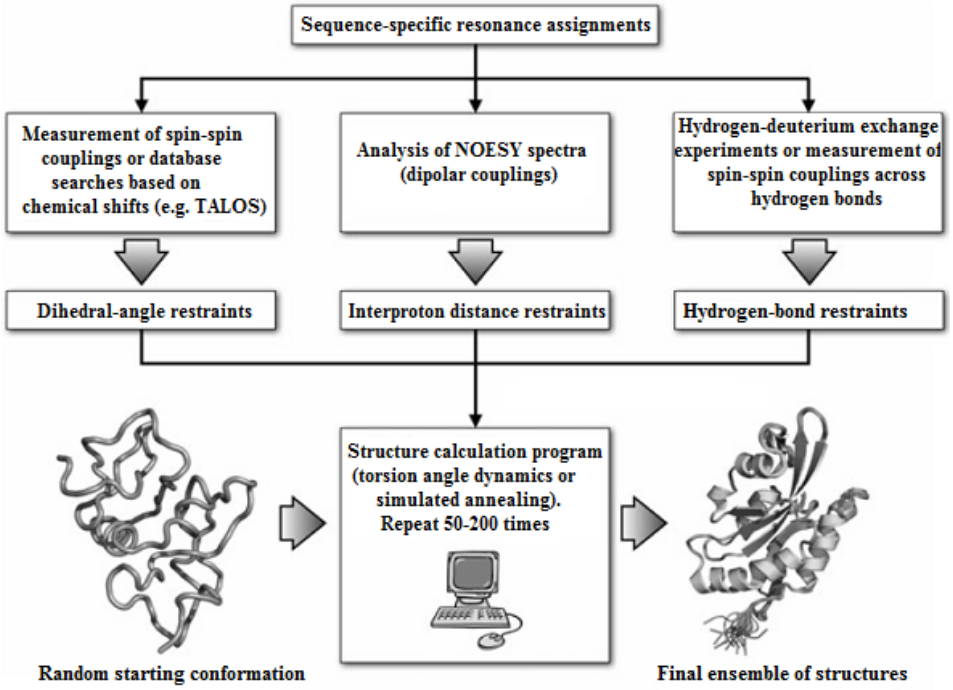

Figure 10. Overview of the process of macromolecular structure determination using NMR spectroscopy (Kwan *et al*., 2011).

However, the distance restraints are not precise enough to give a unique model. Therefore, NMR produces a family of structures, each member satisfying the distance restraints approximately equally well (Kwan *et al*., 2011).

2.3.3. Cryo-EM

Cryo-EM microscopy is a form of transmission electron microscopy where the frozen sample is studied at cryogenic temperatures under vacuum. In Cryo-EM, the specimen is embedded in a thin layer of ice and kept at the temperature of liquid nitrogen or liquid helium for the duration of the experiment. Electron microscopy uses a beam of electrons emitted by a source for sample illumination and production of a sample image (Fig. 11). After passing through the specimen, scattered electrons are focused by the electromagnetic lenses of the microscope (Saibil, 2000; Frank, 2001; Milne *et al*., 2013).

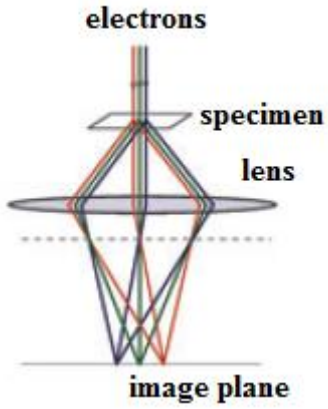

Figure 11. Schematic representation of image formation in an electron microscope (Milne *et al*., 2013).

The resolution is directly influenced by the wavelength of the imaging radiation source (the shorter the wavelength, the higher the attainable resolution). Since electrons have much shorter wavelength compared to visible light, the wavelength of electron radiation does not itself impose a limit on the resolution that may be obtained when imaging biological macromolecules. Why is it not possible to image individual proteins directly in an electron microscope at atomic resolution? This is challenging because electron irradiation leads to breaking of the chemical bonds and creation of free radicals that cause secondary damage of organic matter. Cryo-EM reduces the effects of radiation damage. The main challenge in Cryo-EM is low signal-to-noise ratio, or poor image contrast. The concept of imaging at cryogenic temperatures and the concept of averaging multiple low-dose images form the basis of modern high-resolution biological electron microscopy (Glaeser *et al*., 1971; Frank, 2001; Milne *et al*., 2013).

It is possible to use cryo-electron microscopy for structural studies of large macromolecular complexes intractable by X-ray crystallography or NMR spectroscopy. In contrast to X-ray crystallography Cryo-EM requires much smaller sample amount, poses fewer restrictions on sample purity, and does not require crystallization.

Single-particle cryo-electron analysis is the most commonly used variant of cryo-electron microscopy. In this technique, data from a large number of 2D projection images, featuring identical copies of the specimen under investigation in different orientations, are combined to generate a 3D reconstruction of the structure (Milne *et al*., 2013).

As it is evident from a series of new structures obtained by Cryo-EM at the near atomic resolution: such as ribosomes from human pathogens with the resolution of 3.2 Å (Wong *et al*., 2014) or the strucrute of the yeast mitochondrial large ribosomal subunit with resolution of 3.2 Å (Amunts *et al*., 2014), the development of new detector hardware has led to a resolution revolution in Cryo-EM (Kuhlbrandt, 2014).

2.3.4. SAXS

SAXS is a technique which reveals information about the crystallographic structure, chemical composition, and physical properties of materials and thin films. SAXS allows studying the structure of a variety of non-crystalline objects such as solutions of biological macromolecules, nanocomposites, alloys, synthetic and bio-polymers, organic/inorganic films. SAXS is a technique where the elastic scattering of X-rays by a sample is recorded at very low angles (0.1° – 10°). SAXS probes structure in the nanometer to micrometer range by measuring the scattering intensity at scattering angles close to 0°. SAXS provides structural information on macromolecules between 5 – 25 nm in size. SAXS is used for determination of the microscale or nanoscale structure of particle systems in terms of such parameters as averaged particle sizes, shapes, distribution, and surface-to-volume ratio. SAXS is also able to operate *in situ* and in a time-resolved manner yielding unique information about the kinetics and dynamics of processes (Glatter & Kratky, 1982; Mertens and Svergun, 2010; Petoukhov and Svergun, 2013).

SAXS is used for the low-resolution structural characterization of biological macromolecules in solution. SAXS provides 3D low-resolution structures using *ab-initio* reconstructions and hybrid modeling. In contrast to X-ray crystallography, where structure determination is only possible when the protein of interest is already crystallized, for SAXS the crystallized sample is not needed. Unlike NMR which is limited to the protein size below 40 – 50

kDa, SAXS enables structural studies in a broad range of molecular sizes from small molecules as well as for large multi-molecular assemblies. However, with SAXS it is not possible to measure the positions of the atoms within the molecule. SAXS is often used in combination with high-resolution methods such as X-ray crystallography and NMR. Being complementary to the high-resolution models SAXS low-resolution models can be used for further superimposition with the X-ray or NMR structures (Feigin and Svergun, 1987; Petoukhov and Svergun, 2013).

Until the 1970s, SAXS experiments were done on instruments equipped by laboratory X-ray tubes. Nowadays SAXS is often performed at synchrotron radiation sources. When used to study biological macromolecules, which are typically dispersed in solution, a monochromatic and collimated X-ray beam illuminates macromolecules chaotically oriented in solution. Scattering pattern of these molecules is recorded by an X-ray detector. For dilute solutions, the scattered intensity I is isotropic and depends only on the scattering angle 2θ (Fig. 12).

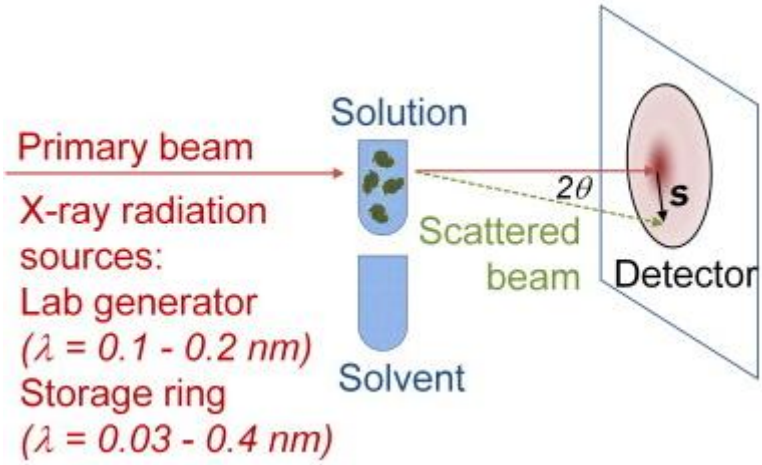

Figure 12. Schematic representation of biological SAXS experiment (with protein molecules in solution) (Petoukhov and Svergun, 2013).

Measurements of the sample containing the protein are complemented by those of the blank solvent (the buffer in which the protein is diluted) and the

latter scattering is afterwords substracted from the measured sample intensities. The resulting scattering profile is usually expressed as a function of the momentum transfer:

$$s = 4\pi \sin(\theta)/\lambda$$

where 2θ is the scattering angle, and λ is the wavelength. Representing the resulting scattering profile the function of the momentum transfer is proportional to the scattering from a single particle averaged over all orientations as well as to the solute concentration. So, SAXS is used to determine the structure of a particle in terms of the average particle size and shape (Petoukhov and Svergun, 2013). X-ray scattering curve (intensity versus scattering angle) is used to create a low-resolution SAXS model of a protein *ab-initio* using bead modeling algorithm implemented in the programs DAMMIN (Svergun, 1999) and DAMMIF (Franke and Svergun, 2009).

3. Materials and methods

3.1. Preparation of protein samples

For structural studies we purified the truncated version of native and selenomethionine-substituted FrpD (SeMet FrpD) containing amino acids 43-271 because we found that FrpD protein crystallization might be hampered by the presence of the N-terminal 42 residues (Sviridova *et al.*, 2010). Since FrpD binds the N-terminal segment of the FrpC protein with the very high affinity ($K_D = 2\times10^{-10}$ M) (Prochazkova *et al.*, 2005) we also prepared $FrpD_{43-271}$-$FrpC_{1-414}$ protein complex in order to characterize the FrpD-FrpC interaction. The N-terminal domain of FrpC, corresponding to residues 1-414 ($FrpC_{1-414}$), was obtained by purification of the 42-kDa protein product resulting from the specific, Ca^{2+}-dependent autocatalytic cleavage of the peptide bond between Asp414 and Pro415 of the purified $FrpC_{1-862}$ protein construct (Osicka *et al.*, 2004; Matyska-Liskova *et al.*, 2016).

All protein samples were purified using a combination of different chromatography techniques (such as nickel affinity chromatography, ion-exchange chromatography and gel-filtration) as described below (Sviridova *et al.*, 2010; Bumba *et al.*, 2012). Purity and integrity of the protein samples were verified by sodium dodecyl sulfate polyacrylamide gel electrophoresis (SDS-PAGE). Protein concentrations were determined by the Bradford assay using bovine serum albumin as a standard (Bradford, 1976).

3.1.1. Purification of native and SeMet $FrpD_{43-271}$

Native $FrpD_{43-271}$ was expressed in *Escherichia coli* (*E. coli*) BL21(λDE3) transformed by *pET28b-frpD*$_{229}$ vector (Sviridova *et al.*, 2010) and grown at 37 °C in a MDO medium supplemented with 60 μg/ml kanamycin to the optical density (OD) of 0.6 at 600 nm. The overexpression of FrpD protein was induced by addition of 1 mM isopropyl β-$_D$-1-thiogalactopyranoside (IPTG). After induction, the bacterial culture was grown for 4 hours at 37°. Cells were centrifuged for 30 min at 5,000 g, resuspended in phophate buffered saline (PBS) buffer, disrupted by sonication on ice using Misonix 3000 sonicator, and the homogenate was centrifuged at 20,000 g at 4 °C for 30 min. The supernatant after cell disruption was loaded on a Ni-Sepharose 6 Fast Flow column, washed with 50 mM imidazole in PBS buffer, and the protein was eluted by 200 mM imidazole in PBS buffer. Collected fractions were pooled,

mixed with the tobacco-etch virus (TEV) protease (1:30 w/w), and dialyzed at 4 °C overnight against a buffer containing 20 mM Tris-HCl (pH 7.4), 150 mM NaCl. The dialyzed sample was loaded on Ni-Sepharose 6 Fast Flow column, and unbound $FrpD_{43\text{-}271}$ protein was collected as flow-through fraction in 20 mM Tris-HCl (pH 7.4), 150 mM NaCl. The protein was concentrated and loaded on Ultrapack TSK G-2000 SWG gel permeation column equilibrated with a buffer containing 10 mM Tris-HCl (pH 7.4), 150 mm NaCl and 0.01% NaN_3. The eluted native $FrpD_{43\text{-}271}$ protein was concentrated with Amicon YM10 ultrafiltration membrane to the 10 mg/ml, and stored at 4 °C.

In order to solve the phase problem by SAD the SeMet $FrpD_{43\text{-}271}$ protein was expressed in *E. coli* BL21(λDE3) from *pET28b-frpD*$_{229}$ vector (Sviridova *et al.*, 2010) using a modified protocol (Van Duyne *et al.*, 1993; Sviridova *et al.*, 2010). The SeMet $FrpD_{43\text{-}271}$ protein was purified from the supernatant after cell disruption following the same protocol as for the native $FrpD_{43\text{-}271}$ protein with the exception that 5 mM β-mercaptoethanol was added to all buffers. The purified SeMet $FrpD_{43\text{-}271}$ was concentrated to the 12 mg/ml, and stored at 4 °C.

3.1.2. Purification of ^{15}N, ^{15}N and ^{13}C isotope-labeled $FrpD_{43\text{-}271}$

$FrpD_{43\text{-}271}$ was expressed in *E. coli* BL21(λDE3) grown at 37 °C in M9 minimal medium supplemented with 60 μg/ml kanamycin and containing either $^{15}NH_4Cl$ for single (^{15}N) labeling or $^{15}NH_4Cl$ and ^{13}C glucose for double (^{15}N and ^{13}C) labeling. The cells were cultivated to OD of 0.6 at 600 nm before 1 mM IPTG was added to induce FrpD synthesis for additional 4 h at 37 °C. Cells were centrifuged for 30 min at 5,000 g, resuspended in PBS buffer, disrupted by sonication on ice, and the homogenate was centrifuged at 20,000 g at 4 °C for 30 min. The supernatant was loaded on a Ni-Sepharose 6 Fast Flow column, washed with 50 mM imidazole in PBS buffer, and the protein was eluted by 200 mM imidazole in PBS buffer. Collected fractions were pooled, mixed with the TEV protease (1:30 w/w), and dialyzed at 4 °C overnight against a buffer containing 20 mM Tris-HCl (pH 7.4), 150 mM NaCl. The dialyzed sample was loaded on Ni-Sepharose 6 Fast Flow column, purification was performed and unbound $FrpD_{43\text{-}271}$ protein was collected as flow-through fraction in 20 mM Tris-HCl (pH 7.4), 150 mM NaCl. The protein was concentrated and loaded on Ultrapack TSK G-2000 SWG gel permeation column equilibrated with a buffer

containing 10 mM Tris-HCl (pH 7.4), 150 mm NaCl. The eluted protein was concentrated with Amicon YM10 ultrafiltration membrane to the 10 mg/ml, and stored at 4 °C.

3.1.3. Purification of the $FrpD_{43-271}$-$FrpC_{1-414}$ complex

Recombinant $FrpC_{1-414}$ protein was purified as 42-kDa fragment of the Ca^{2+}-dependent cleavage of the purified $FrpC_{1-862}$ construct (Osicka *et al.*, 2004; Matyska Liskova *et al.*, 2016). The $FrpC_{1-862}$ protein was expressed in *E. coli* BL21(λ DE3) grown at 30 °C in LB medium supplemented with ampicillin (150 μg/ml) after induction of the cells by 1 mM IPTG. After induction, the bacterial culture was grown for 4 hours grown at 30 °C. Then cells were washed twice in TN buffer (50 mM Tris-HCl, pH 7.4, 150 mM NaCl) supplemented with 5 mM EDTA, resuspended in TN buffer and disrupted by sonication on ice. The cell lyzate was cleared at 20,000 *g* for 30 min and loaded on a Ni-Sepharose equilibrated with TN buffer. The column was extensively washed with TN buffer supplemented with 30 mM imidazole and the $FrpC_{1-862}$ protein was eluted with TN buffer containing 200 mM imidazole. The eluted fractions were collected and supplemented with dithiothreitol (DTT) to a final concentration of 10 mM before the mixture was dialyzed overnight at 4 °C in TN buffer containing 10 mM DTT and 10 mM $CaCl_2$. Addition of Ca^{2+} ions induced the autocatalytic cleavage of $FrpC_{1-862}$ into two protein products ($FrpC_{1-414}$ and $FrpC_{415-862}$) without the cross-linking activity of $FrpC_{1-414}$ due to the presence of DTT. The protein mixture was supplemented with urea to a final concentration of 8 M and loaded on Q-Sepharose equilibrated with 50 mM Tris-HCl (pH 7.4) and 8 M urea. $FrpC_{1-414}$ was recovered from the column in the flow through fraction and concentrated by ultrafiltration (Amicon, 10K membrane). The denatured $FrpC_{1-414}$ was refolded by rapid dilution in buffer containing 50 mM Tris-HCl (pH 7.4), 150 mM NaCl, 2 mM $CaCl_2$. Then the recovered sample was concentrated and loaded on Ultrapack TSK G-2000SWG gel permeation column equilibrated with a buffer containing 50 mM Tris-HCl (pH 7.4), 150 mM NaCl, 2 mM $CaCl_2$. The eluted $FrpC_{1-414}$ protein was concentrated and mixed with the previously purified native $FrpD_{43-271}$ (produced as described in § 3.1.1.) in the ratio 1:1. Then the gel filtration of the

complex was performed. The eluted $FrpD_{43-271}$-$FrpC_{1-414}$ complex was concentrated to the 12 mg/ml, and stored at 4 °C.

3.2. Crystallization of native and SeMet FrpD

Initial screening for crystallization was performed at both 4 and 20 °C by the sitting drop vapor diffusion method using different commercial crystallization screens. Crystallization experiments were setup using freshly purified samples of the native and SeMet $FrpD_{43-271}$ protein at a concentration 5-12 mg/mL. Diffraction-quality crystals of native and SeMet $FrpD_{43-271}$ protein were obtained by vapor diffusion in the sitting drop mode as described in § 4.1 (Sviridova *et al.*, 2010).

Colorless hexagonal-shaped crystals of native $FrpD_{43-271}$ protein were grown at 20 °C from a protein (10 mg/mL in 10 mM Tris-HCl pH 7.4, 150 mM NaCl, 0.01% NaN_3) mixed with precipitant solution containing 0.1 M Tris-HCl pH 8.5 and 2 M ammonium sulfate in 0.6-1 μL sitting drops equilibrated over 50 μL of reservoir solution.

Single crystals of SeMet $FrpD_{43-271}$ protein were obtained at 20 °C by mixing 1 μL of protein (7-9 mg/mL in 10 mM Tris-HCl pH 7.4, 150 mM NaCl, 0.01% NaN_3 and 5 mM β-mercaptoethanol) with 1 μL of reservoir solution (0.1 M Tris-HCl buffer pH 8.5, 20 % (w/v) PEG 8000, 20 % (v/v) PEG 400, and 0.1 M $MgCl_2$) and equilibration over 700 μL of reservoir solution.

3.3. X-ray structure determination of native and SeMet FrpD

Native and SAD data were collected without any additional cryoprotection at 100 K at beamlines MX 14.1 (Fig. 13) and 14.2 of Berlin Electron Storage Ring Society for Synchrotron Radiation (BESSY) (Berlin, Germany) (Mueller *et al.*, 2012).

All diffraction data were processed and scaled using the HKL-3000 software package (Minor *et al.*, 2006; Schneider and Sheldrick, 2002; Terwilliger, 2003). The merohedral twinning was excluded by analysis of cumulative intensity distribution using Padilla-Yeates algorithm (Padilla & Yeates, 2003). Crystal parameters and data collection statistics are summarized in Table 1 of § 4.3. The diffraction data for the native FrpD crystals were collected to a resolution of 2.3 Å using the wavelength of 0.918 Å. For the

SeMet FrpD protein, two datasets were collected. The dataset used for SAD phasing (denominated SeMet1 in Table 1 of § 4.3) was collected at 0.979 Å and the crystal diffracted X-rays to a d_{min} of 2.0 Å. The dataset yielding the resolution of 1.4 Å (denominated SeMet2 in Table 1 of § 4.3) was collected at the wavelength of 0.9184 Å. Diffraction properties of crystal were significantly improved by crystal annealing procedure, which was performed by blocking the cryostream for 3 s.

Figure 13. An image of the Bessy mx BL 14.1 experimental station instrumentation (Mueller *et al.*, 2012).

The crystal structure of the SeMet FrpD protein was determined by SAD utilizing the anomalous signal from selenium atoms. All procedures for phasing and phase improvement by density modification were carried out using the HKL-3000 software package (Minor *et al.*, 2006; Schneider and Sheldrick, 2002; Terwilliger, 2003). Phasing statistics are summarized in Table 1 of § 4.3. The initial model, containing 95% of all residues, was constructed automatically by ARP/wARP (Perrakis *et al.*, 1999) using the electron density maps after density modification with the program DM (Cowtan, 1999). The electron density was well defined and connected for the entire protein, with the exception of the one N-terminal and four C-terminal residues, which could not

be located in the electron density. Structure was refined to 1.4 Å using the high-resolution dataset of SeMet FrpD.

The crystal structure of native FrpD was solved by molecular replacement using the program MOLREP (Vagin and Teplyakov, 2000). Model refinement was carried out using the program REFMAC v. 5.5.01.09 (Murshudov *et al.*, 2011) from the CCP4 package (Winn *et al.*, 2011), interspersed with manual adjustments using Coot (Emsley *et al.*, 2004). The final steps included TLS refinement (Winn *et al.*, 2001). The refinement statistics are summarized in Table 2 of § 4.3. The quality of the protein models was confirmed with MolProbity (Chen *et al.*, 2010) and PROCHECK (Laskowski *et al.*, 1993).

3.4. Identification of the FrpD/FrpC$_{1\text{-}414}$ binding interface using NMR

For preparation of the the FrpD-FrpC$_{1\text{-}414}$ complex, the ^{15}N-labeled FrpD (purified as described in § 3.1.2.) was mixed with the unlabeled FrpC$_{1\text{-}414}$ (purified as described in § 3.1.3.) in a molar ratio of 1:1 and the mixture was loaded on Superdex 200 HR gel filtration column equilibrated with 5 mM sodium phosphate (pH 7.2), 50mM NaCl. The complex was concentrated by ultrafiltration and the sample consisting of 450 µl of 0.5 mM protein, 10% D_2O and 0.05% NaN_3 was used for the measurement. All NMR data were acquired at 35 °C on a 600 MHz Bruker Avance spectrometer equipped with a triple-resonance (^{15}N/^{13}C/^{1}H) cryoprobe (Fig. 14).

Figure 14. An image of the Bruker Avance III HD, 600 MHz spectrometer (image courtesy of www.uochb.cz).

The 2D and 3D spectra recorded to obtain sequence specific assignments for $FrpD_{43-271}$ were: $^{15}N/^{1}H$ HSQC, $^{15}N/^{13}C/^{1}H$ HNCA, HNCO, HN(CA)CO, HNCACB, and CBCA(CO)NH (Bumba *et al.*, 2012). The 3D spectra were acquired over about 24-96 h, depending on their relative sensitivity. All NMR data were processed using Topspin 2.1 (Bruker) and analyzed using the Sparky (UCSF). Perturbations in the chemical shifts of FrpD after formation of the FrpD/$FrpC_{1-414}$ complex were used to identify the FrpD residues involved in $FrpC_{1-414}$ binding. Comparison of the $^{1}H/^{15}N$ HSQC spectra of the free ^{15}N-labeled FrpD and the ^{15}N-labeled FrpD complexed with unlabeled $FrpC_{1-414}$ revealed shifts in the positions of FrpD backbone amide signals. Based on our complete sequence-specific backbone resonance assignments of FrpD (Bumba *et al.*, 2012), a minimal shift analysis was employed to quantify the extent of changes in backbone amide signals of FrpD after $FrpC_{1-414}$ binding, which were evaluated as possible $FrpC_{1-414}$ interaction sites by examination of the FrpD crystal structure.

3.5. SAXS of FrpD protein and FrpD-$FrpC_{1-414}$ complex

SAXS patterns of the native FrpD protein and the $FrpD_{43-271}$-$FrpC_{1-414}$ complex were recorded on the beamline X33 EMBL (Fig. 15) on the storage ring DORIS-III (Hamburg, Germany) (Blanchet *et al.*, 2012).

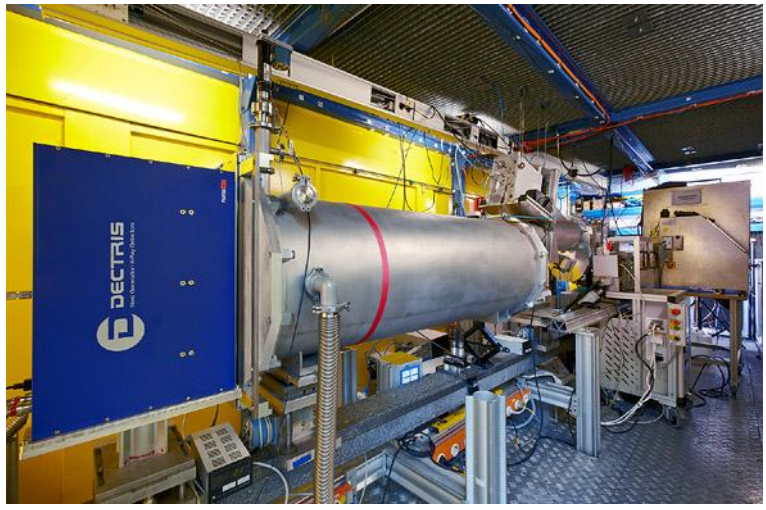

Figure 15. An image of the X33 EMBL beamline (image courtesy of www.embl-hamburg.de).

The protein samples that we used for the SAXS experiments were found to be homogeneous. The native $FrpD_{43-271}$ protein was measured in the concentration range from 1 to 9 mg/ml. The $FrpD_{43-271}$-$FrpC_{1-414}$ complex was measured at three different concentrations ranging from 1 to 5 mg/ml. The data were recorded at room temperature using the pixel 1M PILATUS detector at the sample-detector distance of 2.7 m, and the wavelength λ of 0.15 nm, covering the range of the momentum transfer 0.06 $nm^{-1} < s < 6$ nm^{-1} ($s = 4\pi sin(\theta)/\lambda$, where 2θ is the scattering angle). Each sample was exposed in 8 frames for 15 s to monitor possible radiation damage. The data from corresponding buffers measured before and after each experiment are merged and used as baseline. Bovine serum albumin served as standard with a relative I(0) of 83.93. No radiation damage was observed during the data collection. All data were analyzed using the ATSAS program suite (Petoukhov *et al.*, 2012). The low-resolution shapes of the FrpD protein and FrpD-$FrpC_{1-414}$ complex were reconstructed *ab-initio* with DAMMIF (Franke and Svergun, 2009).

3.6. Comparative analysis of FrpD structure

Crystallographic packing analysis of two crystal forms of FrpD was made using PISA (Krissinel and Henrick, 2007). The analysis of the FrpD secondary structure was made using DSSP (Kabsch and Sander, 1983), ProFunc (Laskowski *et al*., 2005), and Pro-origami (Stivala *et al*., 2011) web servers. Comparative structure-based homology analysis of the FrpD structure was carried out using DALI (Holm & Sanger, 1993), CATH (Orengo *et al*., 1997) and PDBeFold (http://www.ebi.ac.uk/msd-srv/ssm) (Krissinel and Henrick, 2004).

PISA analysis of the crystal-packing parameters indicated the presence of one monomer molecule of the FrpD protein in the asymmetric unit for both hexagonal and primitive orthorhombic crystal forms. Analysis of the protein interfaces did not reveal any specific interactions that could result in a formation of stable quaternary structures for both crystal forms indicating that the biological unit of the FrpD protein is a monomer.

The DALI search for similar three dimensional structures using the refined model of FrpD as a target did not revealed any deposited structures that

are strikingly similar to FrpD. As defined by the DALI, the best fit was obtained for putative uncharacterized Rv0999 ortholog protein from *Mycobacterium smegmatis* (*M. smegmatis*) (PDB code 4TMD; Z-score 5.2; rmsd of 3.8 Å for 114 aligned residues, and sequence identity 9 %). The CATH structural classification search revealed the yeast profilin from *Schizosaccharomyces pombe* (PDB code 3D9Y) (Ezezika *et al*., 2009) as the top candidate. Another structural alignment database search was performed using the protein structure comparison service PDBeFold. The best score was obtained against the chain B (PDB code 3V7B; Z-score 4.7; rmsd of 2.98 Å for 80 aligned residues, and sequence identity 4 %) and chain A (PDB code 3V7B; Z-score 4.6; rmsd of 3.02 Å for 80 aligned residues, and sequence identity 4 %) of DIP2269 protein of unknown function from *Corynebacterium diphtheriae*. Additionally, the structural alignment between FrpD and each of best score candidates using combinatorial extension (Shindyalov and Bourne, 1998) was performed. CE alignment showed low Z-scores (< 4.2) and high rmsd values (> 3.9) for all these candidates.

Taken together the results of comparative structure-based homology analysis of FrpD structure indicated that FrpD fold did not contain the topology sufficiently similar to establish structural homology with other known proteins, indicating that FrpD corresponds to a novel fold.

4. Publications

4.1. Crystallization and preliminary crystallographic characterization of the iron-regulated outer membrane lipoprotein FrpD from *Neisseria meningitidis*

This chapter is based on paper:

Ekaterina Sviridova*, Ladislav Bumba*, Pavlina Rezacova, Katerina Prochazkova, Daniel Kavan, Karel Bezouska, Michal Kuty, Peter Sebo and Ivana Kuta Smatanova. **(2010)** Crystallization and preliminary crystallographic characterization of the iron-regulated outer membrane lipoprotein FrpD from *Neisseria meningitidis*. *Acta Crystallographica Section F*, 66, 1119-1123.

* – equal contribution.

ABSTRACT

Fe-regulated protein D (FrpD) is a *Neisseria meningitidis* outer membrane lipoprotein that may be involved in anchoring of the secreted Repeat in toxins (RTX) protein FrpC to the outer bacterial membrane. However, the function and biological role of the FrpD and FrpC proteins remain unknown. Native and selenomethionine-substituted variants of recombinant $FrpD_{43-271}$ protein were crystallized using the sitting-drop vapor-diffusion method. Diffraction data were collected to the resolution of 2.25 Å for native $FrpD_{43-271}$ protein and to the resolution of 2.00 Å for selenomethionine-substituted $FrpD_{43-271}$ (SeMet $FrpD_{43-271}$) protein. The crystals of native $FrpD_{43-271}$ protein belong to the hexagonal space group $P6_2/P6_4$ while the crystals of SeMet $FrpD_{43-271}$ protein belong to the primitive orthorhombic space group $P2_12_12_1$.

4.2. Backbone resonance assignments of the outer membrane lipoprotein FrpD from *Neisseria meningitidis*

This chapter is based on paper:

Ladislav Bumba, **Ekaterina Sviridova**, Ivana Kuta Smatanova, Pavlina Rezacova, Vaclav Veverka. **(2012)** Backbone resonance assignments of the outer membrane lipoprotein FrpD from *Neisseria meningitidis*. *Biomolecular NMR Assignments*, 8 (1), 53–55.

ABSTRACT

The iron-regulated FrpD protein is a unique lipoprotein embedded into the outer membrane of the Gram-negative bacterium *Neisseria meningitidis*. The biological function of FrpD remains unknown but might consist in anchoring to the bacterial cell surface the Type I-secreted FrpC protein, which belongs to a Repeat in ToXins (RTX) protein family and binds FrpD with very high affinity (K_d = 0.2 nM). Here, we report the backbone ^{1}H, ^{13}C, and ^{15}N chemical shift assignments for the $FrpD_{43–271}$ protein that allow us to characterize the intimate interaction between FrpD and the N-terminal domain of FrpC.

4.3. Structural basis of the interaction between the iron-regulated FrpD and FrpC proteins, putative minor adhesins of *Neisseria meningitidis*

This chapter is based on paper:

Ekaterina Sviridova, Pavlina Rezacova, Alexey Bondar, Vaclav Veverka, Petr Novak, Gundolf Schenk, Dmitri I. Svergun, Ivana Kuta Smatanova, and Ladislav Bumba. Structural basis of the interaction between the iron-regulated FrpD and FrpC proteins, putative minor adhesins of *Neisseria meningitidis*. *Manuscript (prepared for submission to Structure).*

SUMMARY

Iron-regulated protein FrpD is a *Neisseria meningitidis* highly conserved outer membrane lipoprotein of unknown function. It has been hypothesized that the biological function of FrpD might consist in anchoring to the bacterial cell surface the secreted FrpC protein, which belongs to the Repeat in ToXins protein family and binds FrpD with very high affinity (K_D = 0.2 nM). Here, we report the first crystal structures of the native and SeMet derivative FrpD protein as well as low resolution solution structures of FrpD and the FrpD-$FrpC_{1-414}$ complex. The crystal structures of FrpD protein reveal a novel protein fold based on three central β sheets, flanked by three short helices and one long C-terminal α helix. We show the structure-function relationships underlying the mechanism of interaction between the FrpD and FrpC proteins and test the putative function of the FrpD-$FrpC_{1-414}$ complex *in vitro*. Finally, we propose the putative function of the FrpD-$FrpC_{1-414}$ complex as a new minor adhesin of *N. meningitidis*, which mediates the bacterial adhesion to the host epithelial cells and facilitate the colonization.

5. Conclusions

The global goal of our research was to determine the mechanism of *N. meningitis* virulence. In order to address this question we performed comprehensive structural characterization of the iron-regulated protein FrpD and its binding partner FrpC, which likely take part in the early stages of establishing the *N. meningitidis* virulence.

We first determined the structure of the FrpD protein. Since FrpD does not possess significant sequence homology to any proteins with the known structure, we used experimental phasing to determine the structure of FrpD. In order to do it we produced crystals of SeMet FrpD protein and subjected it to the SAD technique measurements. Crystals of native and SeMet FrpD protein suitable for X-ray diffraction experiment were both grown using sitting drop vapor diffusion method in two different newly discovered precipitant compositions. Based on obtained diffraction data crystal structures of native and SeMet FrpD protein were determined to the resolutions 2.3 Å and 1.40 Å, respectively. Crystal structure of SeMet FrpD protein was solved by the SAD method utilizing the anomalous signal from selenium atoms. This solved SeMet FrpD structure was used as a model for molecular replacement of the native FrpD structure.

The first crystal structures of the native and SeMet derivative FrpD protein from *N. meningitidis* were solved from the hexagonal and primitive orthorhombic crystal forms. PISA analysis of the crystal-packing parameters indicated the presence of one monomer molecule of FrpD protein in the asymmetric unit for both crystal forms.

Crystallographic analysis of native and SeMet FrpD proteins revealed that the $FrpD_{43\text{-}271}$ structure has a bean-like shape and it is characterized by the C-terminal α helix traversing a series of antiparallel β strands. The fold of FrpD resembles a compact bean-shaped structure slightly concaved from one side. Atomic coordinates and experimental structure factors of native and SeMet FrpD proteins were deposited in the PDB under the accession codes 5EDJ and 5EDF.

Comparative structure-based FrpD protein folding analysis indicated that FrpD has a unique fold. The fold of FrpD resembles a bean-shaped structure slightly concaved from one side. The closest structural relative of FrpD is the uncharacterized Rv0999 ortholog protein (PDB code 4TMD; Z-score 5.2; rmsd

of 3.8 Å for 114 aligned residues, and sequence identity 9 %) from the Gram-positive bacterium *M. smegmatis*. Performed CE alignment showed low Z-score (< 4.2) and high rmsd value (> 3.9) for this candidate. Taken together these results indicated that *M. smegmatis* Rv0999 ortholog protein fold did not contain the topology sufficiently similar to establish structural homology with FrpD, indicating that FrpD corresponds to a novel fold. This fold does not have any significant similarity in other groups of proteins and potentially attributes FrpD to a new type of membrane proteins localized in bacterial outer membrane.

NMR study of the FrpD protein showed that FrpD consist of eight distinct regions adopting β structure (His59-Phe65, Ser99-Lys111, Asp138-Lys147, Glu176-Lys181, His191-Lys198, Ala203-Asn209, Tyr220-Ile228, and Thr232-Tyr235) and three well define α helices (Gln124-Arg134, Gly157-Thr162, and Gln247-Phe264). The $^{1}H^{N}$, ^{15}N, $^{13}C'$, $^{13}C^{\alpha}$ and $^{13}C^{\beta}$ chemical shifts for $FrpD_{43-271}$ have been deposited to the BMRB database under accession code 18779.

SAXS study of the FrpD protein revealed that SAXS-based *ab-initio* model of FrpD has an overall shape consistent with the X-ray crystal structure, indicating the FrpD shape seen in the crystal structures is maintained in solution. Moreover, SAXS results confirmed the monomeric state of the FrpD protein suggested by the X-ray data. The SAXS data and the *ab-initio* model of the FrpD protein were deposited into Small Angle Scattering Biological Databank: http://www.sasbdb.org/data/SASDBP4.

We next set out to determine the structure of the FrpD-FrpC protein complex. Our numerous trials to crystallize the $FrpD_{43-271}$-$FrpC_{1-414}$ complex did not provide diffraction-quality crystals. Crystallization of $FrpC_{1-414}$ alone also only led to formation of pseudocrystalline aggregates and salt crystals. Therefore, we identified the $FrpD_{43-271}$ residues involved in $FrpC_{1-414}$ binding using the NMR spectroscopy. We found that the most affected residues are situated in the surface-exposed part of the β sheet I: strands β1 (Phe63, Asp64 and Phe65), loop connecting strands β1 and β2 (Gln66 and Gly67), β2 (Lys69 and Val71), loop between β4 and β5 (Asp96, Ala97), β5 (Tyr98); the C-terminal region of the helix α3 (Phe264) and the C-terminal unstructured tail (Lys270, Lys271, Glu272, Leu274 and Tyr275). Finally, we identified the low-

resolution structure of the FrpD-FrpC$_{1-414}$ complex using SAXS. The SAXS data and the *ab-initio* model of the FrpD-FrpC$_{1-414}$ can be accessed in the Small Angle Scattering Biological Databank: http://www.sasbdb.org/data/SASDBQ4.

Summarizing our findings we propose that the putative function of the FrpD-FrpC$_{1-414}$ complex is to act as a minor adhesin of *N. meningitidis*, which mediates the bacterial adhesion to the host epithelial cells and facilitates the colonization. FrpD serves as a membrane anchor attaching FrpC to the bacterial outer membrane, which is important for FrpC functional activity. In the presence of calcium ions the purified recombinant FrpC undergoes highly-specific processing that resembles protein *trans*-splicing (Osicka *et al.*, 2004). This includes the Ca^{2+}-dependent folding of the SPM of FrpC resulting in the autocatalytic cleavage of the Asp$_{414}$-Pro$_{415}$ peptide bond and covalent linkage of the released carboxyl group of Asp$_{414}$ of FrpC$_{1-414}$ to ε-amino group of a neighboring lysine residue of another molecule (Matyska Liskova *et al*., 2016). We tested the hypothesis whether formation of the FrpD-FrpC$_{1-414}$ complex could be involved *in vitro* in binding of *N. meningitidis* to target cell surface. As expected, FrpC$_{1-414}$ was detected as free protein (42 kDa) in the culture supernatant, as well as in the form of cross-linked products (70-130 kDa) on plasma membrane proteins of the epithelial cells A549 after their incubation with *N. meningitidis*. This result clearly indicates that the freshly-secreted FrpC undergoes protein *trans*-splicing that induces the SPM-mediated release of FrpC$_{1-414}$ into mucosal fluids (42 kDa) and subsequent covalent linkage of the released FrpC$_{1-414}$ on plasma membrane proteins of epithelial cells (70-130 kDa). Hence, the cross-linked FrpC$_{1-414}$ exposed on the cell surface of the host cells could serve as a specific target for the FrpD lipoprotein protruding from the outer membrane of bacterial cells.

In this study we describe the structure of the FrpD protein, its newly identified unique fold and characterize the FrpD/FrpC$_{1-414}$ interaction interface. Based on these data we propose a model of FrpD-FrpC$_{1-414}$ complex localization and functional activity. The cleavage and the cross-linking activity of FrpC suggested that formation of the FrpD-FrpC$_{1-414}$ complex on host cell surface after Ca^{2+}-induced protein *trans*-splicing of freshly-secreted FrpC may represent a conceptually novel adhesion strategy that is used by *N. meningitidis* during colonization of respiratory epithelia. FrpD most likely anchors FrpC to

the outer membrane and allows it to carry out its functions. We propose that the putative function of the FrpD-$FrpC_{1-414}$ complex is to act as a minor adhesin of *N. meningitidis*, which mediates the bacterial adhesion to the host epithelial cells and facilitates the colonization. This study constitutes the first step in clarifying the molecular basis of FrpD-FrpC interaction and sets the base for further investigation of the role of these proteins in the virulence mechanism of *N. meningitidis*.

6. References

Amunts, A., Brown, A., Bai, X., Llacer, J. L., Hussain, T., Emsley, P., Long, F., Murshudov, G., Scheres, S. H. W., Ramakrishnan, V. (2014) Strucrute of the yeast mitochondrial large ribosomal subunit. *Science* **343**, 1485-1489

Anderson, M. S., Glode, M. P., Smith, A. L. (1998) Textbook of pediatric infectious diseases. *W. B. Saunders Co, Philadelphia, Pa*

Asherie, N. (2004) Protein crystallization and phase diagrams. *Methods* **34**, 266-272

Basler, M., Linhartova, I., Halada, P., Novotna, J., Bezouskova, S., Osicka, R., Weiser, J., Vohradsky, J., and Sebo P. (2006) The iron-regulated transcriptome and proteome of *Neisseria meningitidis* serogroup C. *Proteomics* **6**, 6194–206

Bax, A. (1994) Multidimensional nuclear-magnetic-resonance methods for protein studies. *Curr Opin Struct Biol* **4(5)**, 738–744

Bergfors, T., ed. (1999) Protein crystallization: strategies, techniques, and tips. *International University Line, La Jolla Ca*

Blanchet, C. E., Zozulya, A. V., Kikhney, A. G., Franke, D., Konarev, P. V., Shang, W., Klaering, R., Robrahn, B., Hermes, C., Cipriani, F., Svergun, D. I and Roessle, M. (2012) Instrumental setup for high throughput solution scattering at the X33 beamline of EMBL-Hamburg. *J Appl Cryst* **45**, 489–495

Blow, D. M. and Crick, F. H. C. (1959) The treatment of errors in the isomorphous replacement method. *Acta Cryst* **12**, 794–802

Bradford, M. M. (1976) Rapid and sensitive method for the quantitation of microgram quantities of protein utilizing the principle of protein-dye binding. *Anal Biochem* **72**, 248–254

Brunger, A. T. (1992) Free *R* value: A novel statistical quantity for assessing the accuracy of crystal structures. *Nature* **355**, 472–475

Bumba, L., Sviridova, E., Kuta Smatanova, I., Rezacova, P., Veverka, V. (2012) Backbone resonance assignments of the outer membrane lipoprotein FrpD from *Neisseria meningitidis*. *Biomolecular NMR Assignments* **8 (1)**, 53-55

Bumba, L., Masin, J., Macek, P., Wald, T., Motlova, L., Bibova, I., Klimova, N., Bednarova, L., Veverka, V., Kachala, M., Svergun, D. I., Barinka, C., and Sebo, P. (2016) Calcium-driven folding of RTX domain β-rolls ratchets translocation of RTX proteins through Type I secretion ducts. *Mol Cell* **62**, 47–62

Broome, C. V. (1986) The carrier state: *Neisseria meningitidis*. *J Antimicrob Chemother* **18**, 25–34

Capecchi, B., Adu-Bobie, J., Di Marcello, F., Ciucchi, L., Masignani, V., Taddei, A., Rappuoli, R., Pizza, M., and Arico, B. (2005) *Neisseria meningitidis* NadA is a new invasin which promotes bacterial adhesion to and penetration into human epithelial cells. Mol Microbiol **55**, 687–698

Cartwright, K. A., Stuart, J. M., Jones, D. M., Noah, N. D. (1987) The Stonehouse survey: nasopharyngeal carriage of meningococci and *Neisseria lactamica*. *Epidemiol Infect* **99**, 591–601

Chasman, D. (2003) Protein structure: determination, analysis, and applications for drug discovery. *CRC Press*

Chayen, N. E. (1992) Microbatch crystallization under oil – a new technique allowing many small-volume crystallization trials. *Journal of Crystal Growth* **122 (1-4)**, 176–180

Chayen, N. E. (1999) Recent advances in methodology for the crystallization of biological macromolecules. *Journal of Crystal Growth* **198-199**, 649–655

Chen, V. B., Arendall, W. B., Headd, J. J., Keedy, D. A., Immormino, R. M., Kapral, G. J., Murray, L. W., Richardson, J. S., Richardson, D. C. (2010) MolProbity: all-atom structure validation for macromolecular crystallography. *Acta Cryst D* **66**, 12–21

Cowtan, K. (1999) Error estimation and bias correction in phase-improvement calculations. *Acta Cryst D* **55,** 1555–1567

Crystallization, research tools, catalog 18. *Hampton research, Aliso Viejo, Ca* https://hamptonresearch.com/documents/growth_101/21.pdf

DeLano, W. L. (2002) *The PyMOL Molecular Viewer.* http://www.pymol.org.

Dodson, E. (2003) Is it jolly SAD? *Acta Cryst D* **59**, 1958–1966

Drenth, J. (1994) Principles of protein X-ray crystallography. *Springer-Verlag, New York*

Ducruix, A. & Giege, R. (1992) Crystallization of nucleic acids and proteins: a practical approach. *Oxford University Press*

Ducruix, A. & Giege, R. (1999) Crystallization of Nucleic Acids and Proteins: a practical approach 2nd ed. *Oxford University Press*

Dyer, D. W., West, E. P. and Sparling, P. F. (1987) Effects of serum carrier proteins on the growth of pathogenic neisseriae with heme-bound iron. *Infect Immun* **55**, 2171–2175

Emsley, P., and Cowtan, K. (2004) Coot: model-building tools for molecular graphics. *Acta Cryst D* **60**, 2126–2132

Evans, P. and McCoy, A. (2007) An introduction to molecular replacement. *Acta Cryst D* **64**, 1–10

Ezezika, O. C., Younger, N. S., Lu, J., Kaiser, D. A., Corbin, Z. A., Nolen, B. J., Kovar, D. R., Pollard, T. D. (2009) Incompatibility with formin Cdc12p prevents human profilin from substituting for fission yeast profiling: insights from crystal structures of fission yeast profiling. *J Biol Chem* **284**, 2088–2097

Felmlee, T., Pellet, S. & Welch, R. A. (1985) Nucleotide sequence of an *Escherichia coli* chromosomal hemolysin. *J Bacteriol* **163**, 94–105

Feigin, L. A., Svergun, D. I. (1987) Structure analysis by small-angle X-ray and neutron scattering. *Plenum Press, New York*

Forman, S., Linhartova, I., Osicka, R., Nassif, X., Sebo, P., and Pelicic, V. (2003) *Neisseria meningitidis* RTX proteins are not required for virulence in infant rats. *Infect Immun* **71**, 2253–2257

Frank, J. (2001) Cryo-electron microscopy as an investigative tool: the ribosome as an example. *BioEssays* **23**, 725–732

Franke, D. & Svergun, D.I. (2009) DAMMIF, a program for rapid ab-initio shape determination in small-angle scattering. *J Appl Cryst* **42**, 342–346

Garman, E. (1999) Cool data: quantity AND quality. *Acta Cryst D* **55**, 1641–1653

Garman, E. and Murray, J. W. (2003) Heavy-atom derivatization. *Acta Cryst D* **59**, 1903–1913

Garman, E. (2010) Radiation damage in macromolecular crystallography: what is it and why should we care? *Acta Cryst D* **66**, 339–351

Garcia-Ruiz, J. M. (1991) Uses of crystal growth in gels and other diffusing-reacting systems. *Key Eng Mater* **88**, 87–106

Garcia-Ruiz, J. M. (2003) Conterdiffusion methods for macromolecular crystallization. *Methods Enzymol* **368**, 130–154

Glaeser, R. M., Cosslett, V. E. & Valdre, U. (1971) Low temperature electron microscopy: radiation damage in crystalline biological materials. *J Microsc* **12**, 133–138

Glatter, O. & Kratky, O., eds. (1982) Small Angle X-ray Scattering. *Academic Press*

Goebel, W. & Hedgpeth, J. (1982) Cloning and functional characterization of the plasmid-encoded hemolysin determinant of *Escherichia coli*. *J Bacteriol* **151**, 1290–1298

Grifantini, R., Sebastian, S., Frigimelica, E., Draghi, M., Bartolini, E., Muzzi, A., Rapuoli, R., Grandi, G., and Attaro Genco C. (2003) Identification of iron-activated and –repressed Fur-dependent genes by transcriptome analysis of *Neisseria meningitidis* group B. *Proc Natl Acad Sci USA* **100 (16)**, 9542–9547

Grifantini, R., Frigimelica, E., Delany, I., Bartolini, E., Giovinazzi, S., Balloni, S., Agarwal, S., Galli, G., Genco, C., Grandi, G. (2004) Characterization of a novel *Neisseria meningitidis* Fur and iron-regulated operon required for protection from oxidative stress: utility of DNA microarray in the assignment of the biological role of hypothetical genes. *Molecular Microbiology* **54 (4)**, 962–979

Grune, T. (2005) Protein Crystallography. Part II. http://shelx.uni-ac.gwdg.de

Hahn, T. (Ed.) (2002) International tables for crystallography, Volume A: Space-group symmetry. *Kluwer Academic Publishers, Dordrecht*

Hantke, K. (2001) Iron and metal regulation in bacteria. *Curr Opin Microbiol* **4**, 172–177

Hart, C. A., and Rogers, T. R. (1993) Meningococcal disease. *J Med Microbiol* **39 (1)**, 3–25

Hill, D. J., Griffiths, N. J., Borodina, E., and Virji, M. (2010) Cellular and molecular biology of *Neisseria meningitidis* colonization and invasive disease. *Clinical Science*, **118**, 547–564

Holm, L. & Sandler, C. (1993) Protein structure comparison by alignment of distance matrices. *J Mol Biol* **233**, 123–138

Hooft, R. W. W., Vriend, G., Sander, C., Abola, E. E. (1996) Errors in protein structures. *Nature* **381**, 272

Keeler, J. (2005) Understanding NMR spectroscopy. *Wiley, Chichester*

Kendrew, J. C., Bodo, G., Dintzis, H. M., Parrish, R. G., Wyckoff, H. & Phillips, D. C. (1958) A three-dimensional model of myoglobin molecule obtained by X-ray analysis. *Nature* **181**, 662–666

Kleywegt, G. J. (2000) Validation of protein crystal structures. *Acta Cryst D* **56**, 249–265

Kovacs-Simon, A., Titball, R. W., and Michell, S. L. (2011) Lipoproteins of bacterial pathogens. *Infect Immun* **79**, 548–561

Kozin, M. B., and Svergun, D. I. (2001) Automated matching of high- and low-resolution structural models. *J Appl Crystallog.* **34**, 33–41

Krieger, E., Koraimann, G., Vriend, G. (2002) Increasing the precision of comparative models with YASARA NOVA – a self-parameterizing force field. *Proteins* **47**, 393–402

Krissinel, E. & Henrick, K. (2007) Inference of macromolecular assemblies from crystalline state. *J Mol Biol* **372**, 774–797

Kuban, V., Novacek, J., Bumba, L., Zidek, L. (2015) NMR assignment of intrinsically disordered self-processing module of the FrpC protein of *Neisseria meningitidis*. *Biomolecular NMR Assignments* **9**, 435–440

Kuhlbrandt, W. (2014) The resolution revolution. *Science* **343**, 1443–1444

Kukacka, Z., Rosulek, M., Strohalm, M., Kavan, D., Novak, P. (2015) Mapping protein structural changes by quantitative cross-linking. *Methods* **89**, 112–120

Kwan, A. H., Mobli, M., Gooley, P. R., King, G. F. and Mackay J. P. (2011) Macromolecular NMR spectroscopy for the non-spectroscopist. *FEBS Journal* **278**, 687–703

Lander, G. C., Saibil, H. R., Nogales, E. (2012) Go hybrid: EM, crystallography, and beyond. *Current Opinion in Struct Biol* **22**, 627–635

Laskowski, R. A., MacArthur, M. W., Moss, D. S., Thornton, J. M. (1993) PROCHECK: a program to check the stereochemical quality of protein structures. *J Appl Cryst* **26**, 283–291

Laskowski, R. A., Watson, J. D. & Thornton, J. M. (2005) ProFunc: a server for predicting protein fumction from 3D structure. *Nucleic Acids Res* **33**, W 89–W93

Linhartova, I., Bumba, L., Masin, J., Basler, M., Osicka, R., Kamanova, J., Prochazkova, K., Adkins, I., Hejnova-Holubova, J., Sadilkova, L., Morova, J. & Sebo, P. (2010) RTX proteins: a highly diverse family secreted by a common mechanism. *FEMS Microbiol Rev* **34**, 1076–1112

Liu, J., Chen, X., Tan, C., Guo, Y., Chen, Y., Fu, S., Bei, W., Chen, H. (2009) *Invivo* induced RTX toxin ApxIVA is essential for the full virulence of *Actinobacillus pleuropneumoniae*. *Vet Microbiol* **137**, 282–289

Lockwood, E. H., Macmillan, R. H. (1978) Geometric symmetry. *Cambridge University Press*

Malkin, A. J., Kuznetsov, Y. G., Land, T. A., DeYoreo, J. J., McPherson, A. (1995) Mechanisms of growth for protein and virus crystals. *Nat Struct Biol* **2(11)**, 956–959

Matthews, B. W. (1968) Solvent content of protein crystals. *J Mol Biol* **33**, 491–497

Mattick, J.S. (2002) Type IV pili and twitching motility. *Annu Rev Microbiol* **56**, 289–314

Matyska Liskova, P., Fiser R., Macek, P., Chmelik, J., Sykora, J., Bednarova, L., Konopasek, I., Bumba, L. (2016) Probing the Ca^{2+}-assisted π-π interaction during Ca^{2+} dependent protein folding. *Soft Matter* **12**, 531–541

McPherson, A. (1999) Crystallization of Biological Macromolecules. *CSHL Press*

McPherson, A., Kuznetsov, Y. G., Malkin, A., Plomp, M. (2003) Macromolecular crystal growth as revealed by atomic force microscopy. *J Struct Biol* **142(1)**, 32–46

McPherson, A. (2004) Introduction to protein crystallization. *Methods* **34**, 254–265

McRee, D. E. (1999) Practical Protein Crystallography second edition. *Academic Press*

Mertens, H. D. T., Svergun, D. I. (2010) Structural characterization of proteins and complexes using small-angle X-ray solution scattering. *Journal of Structural Biology* **172**, 128–141

Mickelsen, P. A., and Sparling, P. F. (1981) Ability of *Neisseria gonorrhoeae, Neisseria meningitidis*, and commensal *Neisseria* species to obtain iron from transferrin and iron compounds. *Infect Immun* **33**, 555–564

Mickelsen, P. A., Blackman, E. and Sparling, P. F. (1982) Ability of *Neisseria gonorrhoeae, Neisseria meningitidis*, and commensal *Neisseria* species to obtain iron from lactoferrin. *Infect Immun* **35**, 915–920

Milne, J. L. S., Borgnia, M. J., Bartesaghi, A., Tran, E. E. H., Earl, L. A., Schauder, D. M., Lengyel, J., Pierson, J., Patwardhan, A. and Subramaniam, S.

(2013) Cryo-electron microscopy – a primer for the non-microscopist. *FEBS Journal* **280**, 28–45

Minor, W., Cymborowski, M., Otwinowski, Z., Chruszcz, M. (2006) HKL-3000: the integration of data reduction and structure solution – from diffraction images to an initial model in minutes. *Acta Cryst D* **62**, 859–866

Muller, D., Hughes, C. & Goebel, W. (1983) Relationship between plasmid and chromosomal hemolysin determinants of *Escherichia coli*. *J Bacteriol* **153**, 846–851

Mueller, U., Darowski, N., Fuchs, M. R., Forster, R., Hellmig, M., Paithankar, K. S., Puhringer, S., Steffien, M., Zocher, G., Weiss, M. S. (2012) Facilities for macromolecular crystallography at Helmholtz-Zentrum Berlin. *J Synchrotron Radiat* **19(3)**, 442–449

Murshudov, G. N., Vagin, A. A. & Dodson, E. J. (1997) Refinement of macromolecular structures by the maximum-likelihood method. *Acta Cryst D* **53**, 240–255

Murshudov, G. N., Skubak, P., Lebedev, A. A., Pannu, N. S., Steiner, R. A., Nicholls, R. A., Winn, M. D., Long, F., Vagin, A. A. (2011) REFMAC5 for the refinement of macromolecular crystal structures. *Acta Cryst D* **67**, 355–367

Ogata, C. M. (1998) MAD phasing grows up. *Nat Struct Biol* **5**, 638–640

Orengo C., Michie A., Jones, S., Jones, D., Swindells, M., Thornton J. (1997) CATH – a hierarchic classification of protein domain structures. *Structure* **5**, 1093–1108

Osicka, R., Kalmusova, J., Krizova, P., Sebo, P. (2001) *Neisseria meningitidis* RTX protein FrpC induces high levels of serum antibodies during invasive disease: polymorphism of *frpC* alleles and purification of recombinant FrpC. *Infect Immun* **69**, 5509–5519

Osicka, R., Prochazkova, K., Sulc, M., Linhartova, I., Havlicek, V., Sebo, P. (2004) A novel "Clip-and-link" activity of repeat in toxin (RTX) proteins from Gram-negative pathogens. *J Biol Chem* **279**, 24944–24956

Padilla, J., Yeates, T. O. (2003) A statistic for local intensity differences: robustness to anisotropy and pseudo-centering and utility for detecting twinning. *Acta Cryst D* **59**, 1124–1130

Painter, J. & Merritt, E. A. (2006) Optimal description of a protein structure in terms of multiple groups undergoing TLS motion. *Acta Cryst D* **62**, 439–450

Pannu, N. S. and Read, R. J. (1996) Improved structure refinement through maximum likelihood. *Acta Cryst A* **52**, 659–668

Parkhill, J., Achtman, M., James, K. D. et al. (2000) Complete DNA sequence of a serogroup A strain of *Neisseria meningitidis* Z2491. *Nature* **404**, 502–506

Payne, S. M. and Finkelstein, R. A. (1977) Detection and differentiation of iron-responsive avirulent mutants on Congo red agar. *Infect Immun* **18**, 94–98

Perkins-Balding, D., Ratliff-Griffin, M., Stojiljkovic, I. (2004) Iron transport systems in *Neisseria meningitidis*. *Microbiol Mol Biol Rev* **68(1)**, 154–171

Perrakis, A., Morris, R., Lamzin, V. S. (1999) Automated protein model building combined with iterative structure refinement. *Nat Struct Biol* **6**, 458–463

Petoukhov, M. V., Franke, D., Shkumatov, A. V., Tria, G., Kikhney, A. G., Gajda, M., Gorba, C., Mertens, H. D. T., Konarev, P. V. and Svergun, D. I. (2012) New developments in the ATSAS program package for small-angle scattering data analysis. *J Appl Cryst* **45**, 342–350

Petoukhov, M. V., Svergun, D. I. (2013) Applications of small-angle X-ray scattering to biomolecular solutions. *Int J Biochem Cell Biol* **45(2)**, 429–437

Pizza, M., and Rappuoli, R. (2015) *Neisseria meningitidis*: pathogenesis and immunity. *Curr Opin Microbiol* **23**, 68–72

Poulsen, F. M. (2002) A brief introduction to NMR spectroscopy of proteins. http://www.cs.duke.edu/brd/Teaching/Bio/asmb/current/2papers/Intro-reviews/flemming.pdf

Prochazkova, K., Osicka, R., Linhartova, I., Halada, P., Sulc, M., Sebo, P. (2005) The *Neisseria meningitidis* outer membrane lipoprotein FrpD binds the RTX protein FrpC. *J Biol Chem* **280**, 3251–3258

Read, R. J. (2003) New ways of looking at experimental phasing. *Acta Cryst D* **59**, 1891–1902

Rhodes, G. (2006) Crystallography Made Crystal Clear, Third Edition: A Guide for Users of Macromolecular Models (Complementary Science). *Elsevier Inc*

Rouphael, N. G. and Stephens, D. S. (2012) *Neisseria meningitidis*: biology, microbiology, and epidemiology. *Methods Mol Biol* **799**, 1–20

Rosenstein, N. E., Perkins, B. A., Stephens, D. S., Popovic, T., Hughes, J. M. (2001) Meningococcal disease. *N Engl J Med* **344**, 1378–1388

Rubinson, K. A., Ladner, J. E., Tordova, M. and Gilliland, G. L. (2000) Cryosalts: suppression of ice formation in macromolecular crystallography. *Acta Cryst D* **56**, 996–1001

Rupp, B. (2010) Biomolecular crystallography. *Garland Science, Taylor & Francis Group, LLC*

Sadarangani, M., Pollard, A. J., Gray-Owen, S. D. (2011) Opa proteins and CEACAMs: pathways of immune engagement for pathogenic *Neisseria*. *FEMS Microbiol Rev* **35**, 498–514

Sadilkova, L., Osicka, R., Sulc, M., Linhartova, I., Novak, P. & Sebo, P. (2008) Single-step affinity purification using a self-excising module from *Neisseria meningitidis* FrpC. *Protein Sci* **17**, 1834–1843

Saibil, H. R. (2000) Macromolecular structure determination by cryo-electron microscopy. . *Acta Cryst D* **56**, 1215–1222

Sayre, D. (1952) The squaring method: a new method for phase determination. *Acta Cryst* **5**, 60–65

Scapin, G. (2013) Molecular replacement then and now. *Acta Cryst D* **69**, 2266–2275

Scarselli, M., Serruto, D., Montanari, P., Capecchi, B., Adu-Bobie, J., Veggi, D., Rappuoli, R., Pizza, M., Arico, B. (2006) *Neisseria meningitidis* NhhA is a multifunctional trimeric autotransporter adhesin. *Mol Microbiol* **61**, 631–644

Schryvers, A. B., and Stojiljkovic, I. (1999) Iron acquisition systems in the pathogenic *Neisseria*. *Mol Microbiol* **32**, 1117–1123

Schneider, T. R., and Scheldrick, G. M. (2002) Substructure solution with SHELXD. *Acta Cryst D* **58**, 1772–1779

Sheldrick, G. M. and Schneider, T. R. (1997) SHELXL: high-resolution refinement. *Methods Enzymol* **277**, 319–343

Sheldrick, G. M. (2002) Macromolecular phasing with SHELXE. *Z Kristallogr* **217**, 644–650

Shen, Y., Delaglio, F., Cornilescu, G., Bax, A. (2009) TALOS +: a hybrid method for predicting protein backbone torsion angles from NMR chemical shifts. *J Biomol NMR* **44(4)**, 213–223

Shindyalov, I. N., and Bourne, P. E. (1998) Protein structure alignment by incremental combinatorial extension (CE) of the optimal path. *Protein Engineering* **11**, 739–747

Staab, J. F., Bradway, S. D., Fidel, P. L., Sundstrom, P. (1999) Adhesive and mammalian transglutaminase substrate properties of *Candida albicans* Hwp1. *Science* **283**, 1535–1538

Stephens, D. S., Hoffman, L. H., McGee, Z. A. (1983) Interaction of *Neisseria meningitidis* with human nasopharyngeal mucosa: attachment and entry into columnar epithelial cells. *J Infect Dis* **148** (3), 369–376

Stephens, D. S. (1999) Uncloaking the meningococcus: dynamics of carriage and disease. *Lancet* **353**, 941–942

Stephens, D. S., Greenwood, B., Brandtzaeg, P. (2007) Epidemic meningitis, meningococcaemia, and *Neisseria meningitidis*. *Lancet* **369**, 2196–2210

Stephens, D. S. (2009) Biology and pathogenesis of the evolutionary successful, obligate human bacterium *Neisseria meningitidis*. *Vaccine* **27S**, B71–B77

Stivala, A., Wybrow, M., Wirth, A., Whisstock, J. & Stuckey, P. (2011) Automatic generation of protein structure cartoons with Pro-origami. *Bioinformatics* **27 (23)**, 3315–3316

Sutherland, T. C., Quattroni, P., Exley, R. M., and Tang, C. M. (2010). Transcellular passage of *Neisseria meningitidis* across a polarized respiratory epithelium. *Infect Immun* **78**, 3832–3847

Svergun, D. I. (1999) Restoring low resolution structure of biological macromolecules from solution scattering using simulated annealing. *Biophysical Journal* **76**, 2879–2886

Sviridova, E., Bumba, L., Rezacova, P., Prochazkova, K., Kavan, D., Bezouska, K., Kuty, M., Sebo, P., Kuta Smatanova, I. (2010) Crystallization and preliminary crystallographic characterization of the iron-regulated outer membrane lipoprotein FrpD from *Neisseria meningitidis*. *Acta Cryst F* **66**, 1119–1123

Taylor, G. (2003) The phase problem. *Acta Cryst D* **59**, 1881–1890

Terwilliger, T. C. (2000) Maximum-likelihood density modification. *Acta Cryst D* **56**, 965–972

Terwilliger, T. C. (2003) SOLVE and RESOLVE: automated structure solution and density modification. *Methods Enzymol 374*, 22–37

Tettelin, H., Saunders, N. J., Heidelberg, J. *et al.* (2000) Complete genome sequence of *Neisseria miningitidis* serogroup B strain MC58. *Science* **287**, 1809–1815

Thompson, S. A., Wang, L. L., West, A., Sparling, P. F. (1993) *Neisseria meningitidis* produces iron-regulated proteins related to the RTX family of exoproteins. *J Bacteriol* **175**, 811–818

Thompson, S. A., Wang, L. L., West, A. & Sparling, P. F. (1993a) Cloning and nucleotide sequence of frpC, a second gene from *Neisseria meningitidis* encoding a protein similar to RTX cytotoxins. *Mol Microbiol* **9**, 85–96

Thompson, S. A. & Sparling, P. F. (1993b) The RTX cytotoxin-related FrpA protein of *Neisseria meningitidis* is secreted extracellularly by meningococci and by HlyBD+ *Escherichia coli*. *Infect Immun* **61**, 2906–2911

Tzeng, Y. L. & Stephens, D. S. (2000) Epidemiology and pathogenesis of *Neisseria meningitidis*. *Microbes and Infection* **2 (1)**, 687–700

Vagin, A., Teplyakov, A. (2010) Molecular replacement with MOLREP. *Acta Cryst D* **66**, 22–25

Van Duyne, G. D., Standaert, R. F., Karplus, P. A., Schreiber, S. L., Clardy, J. (1993) Atomic structures of the human immunophilin FKBP-12 complexes with FK506 and rapamycin. *J Mol Biol* **229 (1)**, 105–124

Vellieux, F. M. and Read, R. J. (1997) Noncrystallographic symmetry averaging in phase refinement and extension. *Methods Enzymol* **277**, 18–53

Virji, M. (1996) Meningococcal disease: epidemiology and pathogenesis. *Trends in Microbiology* **4 (12)**, 466–469

Volkov, V. V., and Svergun, D. I. (2003) Uniqueness of *ab-initio* shape determination in small-angle scattering. *J Appl Crystl* **36**, 860–864

Wang, B. C. (1985) Resolution of phase ambiguity in macromolecular crystallography. *Methods Enzymol* **115**, 90–112

Weber, P. C. (1991) Physical principles of protein crystallization. *Adv Prot Chem* **41**, 1–36

Weber, P. C. (1997) Overview of protein crystallization methods. *Methods in enzymology* **276**, 13–22

Welch, R. A. (1991) Pore-forming cytolysins of gram-negative bacteria. *Mol Microbiol* **5**, 521–528

Welch, R. A. (2001) RTX toxin structure and function: a story of numerous anomalies and few analogies in toxin biology. *Curr Top Microbiol Immunol* **257**, 85–111

Winn, M. D., Isupov, M. N., Murshudov, G. N. (2001) Use of TLS parameters to model anisotropic displacements in macromolecular refinement. *Acta Cryst D* **57**, 122–133

Winn, M. D., Ballard, C. C., Cowtan, K. D., Dodson, E. J., Emsley, P., Evans, P. R., Keegan, R. M., Krissinel, E. B., Leslie, A. G., McCoy, A., McNicholas, S. J., Murshudov, G. N., Pannu, N. S., Potterton, E. A., Powell, H. R., Read, R. J., Vagin, A., Wilson, K. S. (2011) Overview of the CCP4 suite and current developments. *Acta Cryst D* **67**, 235–242

Wong, W., Bai X., Brown, A., Fernandez, I. S., Hanssen, E., Condron, M., Tan, Y. H., Baum, J., Scheres, S. H. W. (2014) Cryo-EM structure of the *Plasmodium falciparum* 80S ribosome bound to the anti-protozoan drug emetine. *Elife*, 1–20

Young, M. M., Tang, N., Hempel, J. C., Oshiro, C. M., Taylor, E. W., Kuntz, I. D., Gibson, B. W., Dollinger, G. (2000) High throughput protein fold identification by using experimental constraints derived from intramolecular cross-links and mass spectrometry. *Proc Natl Acad Sci USA* **97**, 5802–5806

Zang, K. Y. J., Cowtan, K. D., & Main, P. (2001) Phase improvement by iterative density modification. *International Tables for Crystallography F*, 311–324

sviridova@nh.cas.cz

Integrated structural study of the FrpD protein from *Neisseria meningitidis*
Ph.D. Thesis Series, 2016, No. 5

Printed in the Czech Republic by Typodesign
Edition of 20 copies

University of South Bohemia in České Budějovice
Faculty of Science
Branišovská 1760
CZ-37005 České Budějovice, Czech Republic

Phone: +420 387 776 201
www.prf.jcu.cz, e-mail: sekret-fpr@prf.jcu.cz